

# Scratching the Surface of Unventured Possibilities with In Situ Self-Assembly: Protease-Activated Developments for Imaging and Therapy

Germain Kwek, Thang Cong Do, Xiaoling Lu, Jun Lin, and Bengang Xing\*

Cite This: *ACS Appl. Bio Mater.* 2021, 4, 2192–2216

Read Online

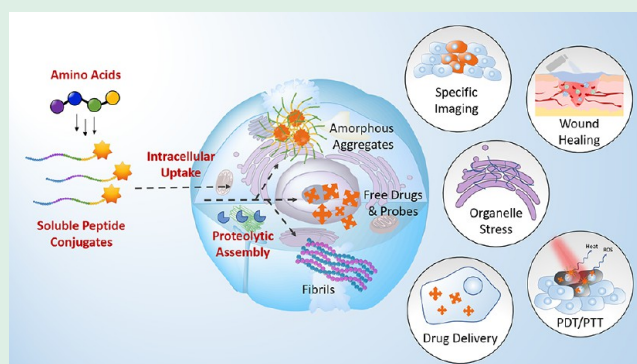
ACCESS |

Metrics & More

Article Recommendations

**ABSTRACT:** In situ self-assembly has attracted increasing research interest for applications in imaging and therapy in recent years. Particularly for protease-activated developments, inspiration is drawn from the innate specificity of their catalytic activities, rapid discovery of the various roles they play in the proliferation of certain diseases, and inherent susceptibility of small molecule peptide conjugates to proteolytic digestion in vivo. The over-expression of a disease-related protease of interest can be exploited as an endogenous stimulus for site-specific self-assembly to largely amplify a molecular event happening at the cellular level. This holds great potential for applications in early stage disease detection, long-term disease monitoring, and sustained therapeutic effects. This review summarizes the recent developments in protease-activated self-assemblies for imaging and therapeutic applications toward the manifestation of tumors, bacterial infections, neurodegenerative disorders, and wound recovery.

**KEYWORDS:** *in situ*, protease-activated, self-assembly, peptide, bio-imaging, therapeutics



## 1. INTRODUCTION

In order to sustain life, living organisms produce a variety of biological building blocks such as lipids, nucleic acids, and amino acids that form more profound and highly organized supramolecular nanostructures with well-defined biological functions through spontaneous self-assembly.<sup>1</sup> Such examples include the cell membrane made up mainly of lipids and proteins maintaining the integrity of cells,<sup>2</sup> the deoxyribonucleic acid (DNA) double helix comprising nucleic acids storing genetic information,<sup>3</sup> and enzymes consisting of amino acids and peptides catalyzing a wide array of vital chemical reactions in the body.<sup>4</sup> Inspired by these self-assembling building blocks of life, self-assembled nanoscale materials have garnered increased research interest in recent years and have been utilized widely in the design of structures for diagnostic<sup>5,6</sup> and therapeutic purposes.<sup>7,8</sup>

A specific category of proteins known as enzymes act as catalysts to accelerate a myriad of chemical reactions in the biological environment with high specificity and efficiency,<sup>9</sup> one of which is self-assembly, an ubiquitous process in life playing various biological roles from maintaining cellular functions and integrity to causing numerous abnormalities in diseases.<sup>10–14</sup> While various research advancements over the years have strived to adopt the use of physical and chemical perturbations to assemble small molecules into supramolecular

nanostructures more efficiently, the assembly of biologically functional nanostructures is still prevalently achieved efficiently and specifically through enzymes in nature. Therefore, compared to physical and chemical perturbations such as ligand receptor interactions and pH and temperature changes, self-assembly activated by specific enzymatic activity is definitely more promising due to its inherent biocompatibility in assimilating the process with biological events.<sup>15,16</sup>

The specificity of an enzyme lies with its ability to recognize and subsequently catalyze the chemical transformation of either a single type of substrate or a group of compounds sharing a common motif. Many natural enzymes have been discovered and studied over the years, most of them catalyzing a defined type of reaction with varying degrees of specificity to their substrates. In order to achieve bioadaptive and site-specific self-assembly with precise superstructure control in a complex living system, the rational design of a precursor

**Special Issue:** Biospecies Sensors

**Received:** October 15, 2020

**Accepted:** December 31, 2020

**Published:** January 12, 2021



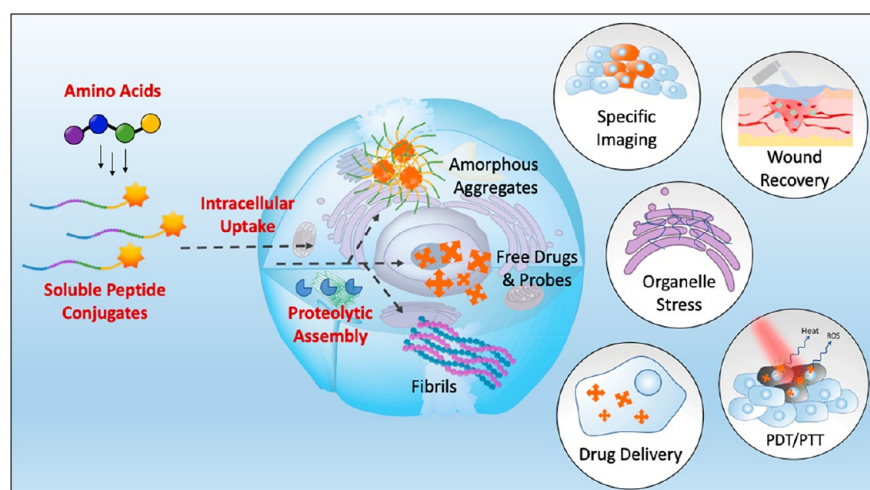


**Figure 1.** Schematic illustration of in situ protease-activated self-assemblies and their potential applications.

(typically either a copy of the enzyme's natural substrate or a derivative of it) that can be specifically recognized and chemically transformed by the enzyme of interest is required. The resulting amphiphilic product of the enzymatic reaction would generally be conferred the tendency to self-aggregate and form more organized nanostructures with better stability.<sup>17</sup>

To date, abundant supramolecular nanostructures formed via enzymatic self-assembly have been developed.<sup>18</sup> Particularly, peptides have been heavily exploited<sup>19–23</sup> as building blocks for self-assembling nanomaterials due to their inherent biocompatibility, ease in design, and vast molecular possibilities made feasible through different amino acid perturbations and available functional groups.<sup>24–28</sup> Synthetic protocols for peptide-based nanostructures are also well-established, such as in solid- and solution-phase peptide synthesis techniques.<sup>29,30</sup>

Even though early in vivo applications of peptide molecules suffer from poor stability due to susceptibility to proteolytic digestion and premature clearance from the living system,<sup>31,32</sup> recent advances have shown promising applications in exploiting this proteolytic susceptibility to generate amphiphilic molecules capable of further self-assembly into more stable hierarchical peptide-based superstructures with improved targeting and therapeutic performance compared to the sole peptide molecule itself.<sup>7</sup> Moreover, peptides naturally adopt well-defined secondary structures such as  $\alpha$ -helices and coiled coils,  $\beta$ -sheets and turns.<sup>17</sup> The formation of  $\alpha$ -helical structures are induced by hydrogen bonding between backbone amides,<sup>33,34</sup> whereas  $\beta$ -sheets mainly consist of alternating hydrophilic and hydrophobic residues permitting hydrogen bonding between carbonyl groups and backbone amides. The presence of  $\pi$ - $\pi$  interactions and complementary ionic bonds are also known to further stabilize  $\beta$ -sheet structures.<sup>35,36</sup> In addition, more diverse peptide-based nanostructures have also been made available through further conjugation of peptides with long alkyl chains to create peptide amphiphiles capable of self-assembly in aqueous solutions.<sup>37</sup> Likewise, large aromatic capping groups such as fluorenyl methoxycarbonyl, naphthalene, and bis-pyrene can also be similarly conjugated to provide more extensive  $\pi$ - $\pi$  interactions, hence promoting self-assembly.<sup>38,39</sup>

Figure 1 illustrates the general process for enzyme-activated self-assembly in the cellular environment. As depicted, the precursors often contain a substrate motif which will be

recognized by a specific proteolytic enzyme of interest. Upon coming into contact with target cells, the protease present will catalyze the transformation of the precursors into amphiphilic products that spontaneously self-assemble via noncovalent interactions (hydrogen bonding,  $\pi$ - $\pi$  interactions, hydrophobic interactions, and charge interactions) into supramolecular nanostructures intracellularly. Even for enzymatic products that are not hydrophobic enough to subsequently self-assemble, Rao and co-workers have designed biocompatible condensation<sup>22</sup> and intracellular macrocyclization<sup>23</sup> reaction strategies capable of controlled nanostructure assembly in living systems. These general strategies can be adapted to be responsive toward a variety of different enzymes and triggers. The resulting aggregation of the enzymatic product can then be used to retain imaging and therapeutic agents at specific sites of upregulated enzymatic activity. Optical and therapeutic effects of the original imaging and therapeutic agent can then be further enhanced due to the added self-assembling properties. Furthermore, the expression levels of different enzymes vary in differing conditions and environments depending on the type of cells including tumor or nontumor, and where the cells are located within the body. Enzyme-activated self-assembly thus empowers researchers with the ability to control delivery, response, and functions of the assembled supramolecular nanostructures.<sup>17</sup> These structures can then be utilized to accurately and precisely report the health status of the body for early disease diagnosis and subsequent monitoring of the recovery process. Additionally, these structures can also be further adapted to provide multimodal treatment as well.

Several comprehensive reviews regarding self-assembled peptide-based nanomaterials for biomedical imaging and therapy,<sup>7,17</sup> nanodrug delivery systems, and disease-related molecular imaging and theranostics<sup>5</sup> have already been published. However, there is a lack of comprehensive reviews focusing on protease-activated assembly systems, which have seen a surge in research interest over the years. In this review, we will mainly focus on the developments in in situ protease-activated self-assemblies. We will discuss their applications in imaging and therapy, followed by perspective outlooks for future developments.

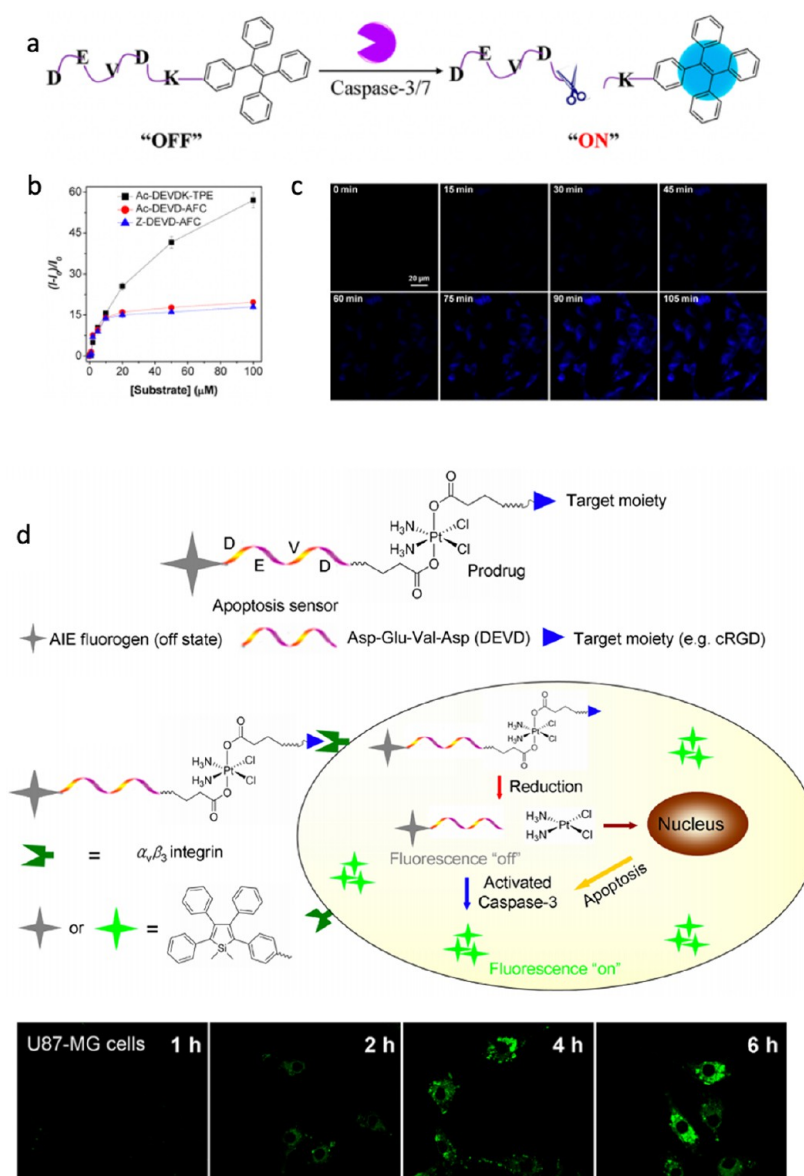


**Figure 2.** (a) Schematic illustration of AIE probe for caspase activity studies. (b) Enhanced fluorescence response of AIE probe compared to commercial coumarin-based probes. (c) Real-time fluorescence images showing the cell apoptotic process. Panels a–c reproduced with permission from ref 62. Copyright 2012 American Chemical Society. (d) Schematic illustration of the targeted theranostic platinum(IV) prodrug with a built-in AIE light-up apoptosis sensor for non-invasive in situ early evaluation of its therapeutic responses and real-time CLSM images displaying the apoptotic progress. Reproduced with permission from ref 64. Copyright 2014 American Chemical Society.

## 2. PROTEASE-ACTIVATED SELF-ASSEMBLIES FOR IMAGING

Aberrant dysregulation of certain enzymes are often correlated with the manifestation of diseases such as tumors and bacterial infections. This abnormality often occurs way before the onset of observable symptoms.<sup>40,41</sup> Therefore, the overexpression of a certain enzyme of interest can be exploited as a trigger to activate the self-assembling properties of a responsive nanoprobe. Upon activation, the specific aggregation and accumulation of the active nanoprobe can be utilized for early stage disease diagnosis and also subsequent evaluation of the administered treatment thereafter.

Xu and co-workers were the pioneers of enzyme-induced self-assembly (EISA). Their work over the years has mainly exploited the overexpression of phosphatases in disease-infected environments as triggers to widely develop con-

struction of short-peptide-based nanomaterials in situ for therapeutic and imaging purposes.<sup>42–47</sup> Typically, functional molecules such as therapeutic agents and fluorescence probes are co-assembled or conjugated with precursors of self-assembling motifs. Upon successful enzymatic dephosphorylation, the perturbation in the hydrophilic–hydrophobic balance of the molecules causes them to self-aggregate into supramolecular structures with not only greater stability but also enhanced optical and therapeutic effect.

Following their success with phosphatase-like enzymes, there has been an increased interest in the adaptation of the EISA strategy to other types of enzymes, particularly proteases due to the high susceptibility of peptides to proteolytic digestion in vivo. Proteases are among the most diverse and largest groups of enzymes, representing almost 2% of the human genome.<sup>48</sup> They are a class of enzymes that irreversibly catalyze the

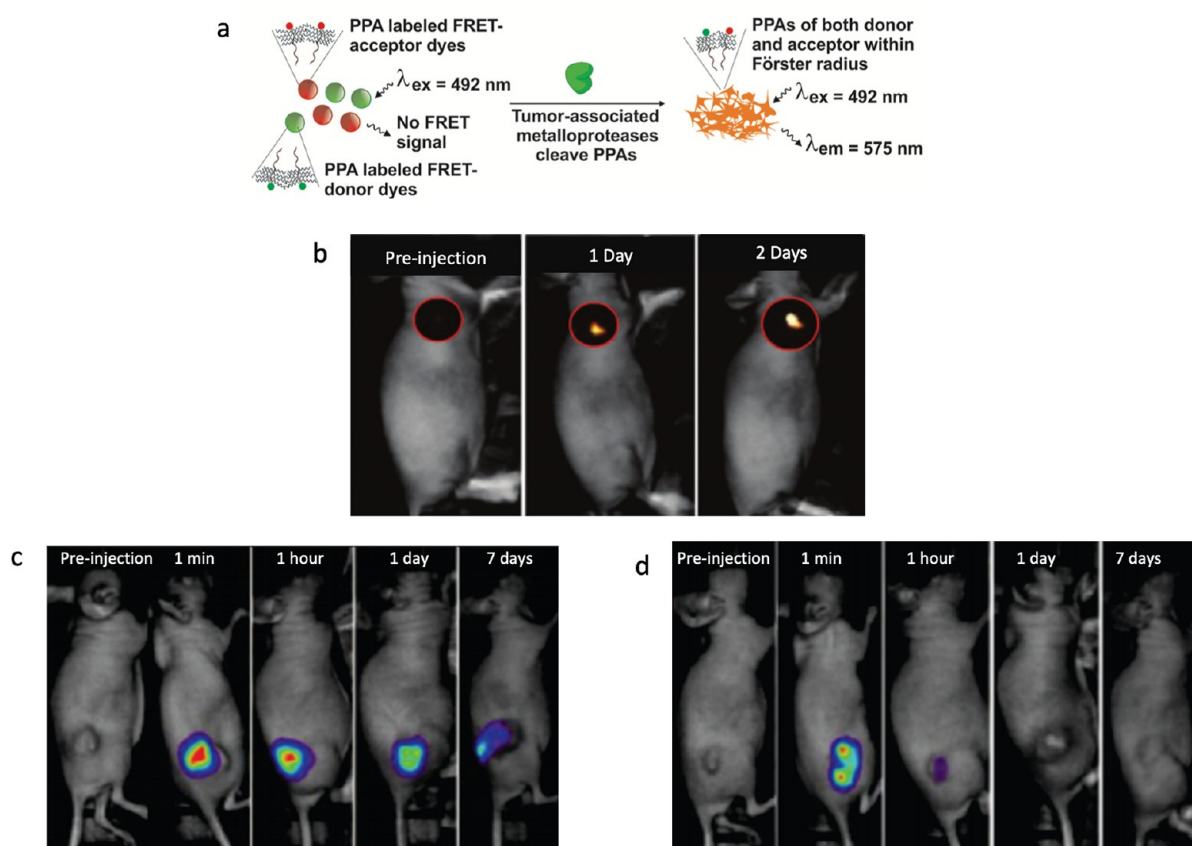


**Figure 3.** (a) General scheme for enzyme-directed accumulation and retention of nanoparticle probes based on dye-labeled peptide–polymer amphiphiles. (b) Intravenously injected mice imaged to show the time course accumulation of enzyme-responsive particles in the tumor region. Reproduced with permission from ref 70. Copyright 2013 Wiley-VCH. (c) Intratumoral injection to determine relative levels of retention of enzyme-responsive nanoparticles vs (d) control particles with HT-1080 tumors. Reproduced with permission from ref 72. Copyright 2013 American Chemical Society.

breaking down of amide bonds in proteins to smaller polypeptides or single amino acids,<sup>49</sup> playing vital roles in virtually all biological processes.<sup>50</sup> However, dysregulations of various proteases have also been found to be correlated to the progression of diseases such as cancer,<sup>51–53</sup> bacterial infections,<sup>54</sup> and neurodegenerative disorders.<sup>55</sup> Intuitively, these disease-associated proteases have been heavily exploited as promising therapeutic targets for the activation of a wide variety of prodrugs due to the innate substrate specificity of their proteolytic active site.<sup>56,57</sup> Compared to enzymes responsive toward specific functional groups such as phosphatase and esterase, proteases have well-characterized catalytic activities, as well as the ability to more specifically and selectively cleave substrates containing unique amino acid sequences that are specially tailored to the architecture of their different proteolytic active sites. As such, various versatile peptide sequences have been frequently employed as bioactive linkers to allow for targeted and site-specific delivery of a wide array of cargo such as therapeutic agents, photosensitizers, and fluorescent dyes.<sup>56–58</sup> Multiple protease-labile conjugates based on this highly adaptive platform have been developed<sup>48</sup> and are currently used in certain clinical treatments.<sup>59,60</sup>

**2.1. Tumor Imaging.** Tumor imaging is an important technique that not only aids the visualization but also the study and characterization of tumors in a living system at cellular and molecular levels. It plays a vital and indispensable role toward the accuracy of tumor diagnostics and precision of the

administered therapy. Upregulated proteolytic activities unique to the manifestation of certain tumors have been recently exploited as a rising strategy for activating spontaneous assembly of nanomaterials as contrast agents to more effectively image tumors with prolonged retention at sites of interest, enhanced specificity, and improved signal-to-noise ratio.

Many toxicants, as well as most compounds used for tumor treatment, are known to induce cellular apoptosis, a form of programmed cell death. Therefore, factors influencing apoptosis often affect the outcome of the administered therapy as well.<sup>17</sup> Caspases are a class of proteolytic enzymes well-known as the executioners of cellular apoptosis, in which its activation would lead to cleavage of critical cellular substrates such as lamins and poly(ADP-ribose) polymerase (PARP), causing the affected cells to undergo a dramatic morphological change in order to prevent inducing an immune response.<sup>61</sup> The detection of caspase activities would hence be able to provide valuable insights into the evaluation of both disease progression and efficiency of the treatment administered. Liu and co-workers designed a cell permeable fluorescent probe capable of aggregation-induced emission (AIE) for real-time apoptosis imaging<sup>62</sup> (Figure 2a). The AIE probe consisting of a hydrophilic caspase-responsive peptide (DEVD)<sup>63</sup> and a hydrophobic tetraphenylethene (TPE) fluorogen with AIE properties was initially nonfluorescent in aqueous solutions. Upon cellular apoptosis, the activation of caspase-3/-7 would

cleave the enzyme-responsive peptide substrate, activating fluorogenic performances that supersede that of commercial coumarin-based probes (Figure 2b). The enhanced performance was attributed to the population of the radiative decay channels, caused by the added aggregation ability of released TPE residues with restricted intramolecular rotations. The designed probe not only enabled the detection of caspase activities but also opened up an avenue for real-time observation of apoptotic progress in living cells due to AIE (Figure 2c). This work has validated the superiority of molecular self-assembly in enhancing the optical effect of fluorescent molecular probes by simply using an AIE to boost the signal-to-noise ratio. Subsequently, the same group then went on to extend their AIE detection strategy to further develop non-invasive real-time monitoring of drug-induced apoptosis to evaluate the therapeutic efficacy of a conjugated anticancer platinum(IV) prodrug<sup>64</sup> (Figure 2d). Nonetheless, continuous efforts have also been made in adapting the strategy to develop AIE probes responsive toward another tumor-related proteolytic enzyme, cathepsin B. Cathepsin B is a lysosomal protease aberrantly upregulated in many kinds of tumors,<sup>65</sup> thus frequently exploited as a target for enzyme-responsive drug delivery.<sup>66,67</sup> Likewise, AIE fluorescent probes responsive toward the proteolytic activity of cathepsin B were similarly conjugated to a prodrug<sup>68</sup> to allow for targeted and image-guided therapeutics. Intriguingly, Liu and co-workers incorporated dicyanovinyl groups to cathepsin B-responsive TPE fluorogens and successfully obtained aggregations of photosensitizers that could efficiently generate reactive oxygen species (ROS) upon irradiation.<sup>69</sup> Despite its limitation in having short excitation wavelengths, impeding subsequent practical applications until further molecular developments to increase the absorption wavelengths of AIE fluorogens, it is no doubt that the work demonstrated the potential possibility of dual-functional probes with both activatable photoactivity and fluorescence for image-guided photodynamic therapy.

On the other hand, Gianneschi and co-workers proposed an alternative strategy for enzyme-triggered retention and active accumulation of nanoprobe in vivo by virtue of a supra-molecular self-assembly event, where the nanoprobe are chemically altered to form slow clearing morphologies within tumors<sup>70</sup> (Figure 3a). Matrix-metalloproteinases (MMPs) are an extensively studied class of secreted and membrane-bound proteases due to their role and overexpression in various tumors.<sup>71</sup> Upregulated MMP-2/-9 activities in tumors were chosen as stimuli in particular due to their unique capabilities in transmitting signals in vivo via catalytic amplification. The group designed peptide-polymer amphiphiles (PPAs) consisting of MMP-2/-9 peptide recognition sequences conjugated to form brush copolymers. In addition, the PPAs were also terminally labeled with donor or acceptor dyes. When dialyzed from dimethyl sulfoxide (DMSO) into buffered water subsequently, the PPAs formed fluorescent spherical micellar nanoparticles with the peptide substrate on the outside as a hydrophilic shell. Upon MMP-specific cleavage of the peptide substrate, the spherical morphologies of the polymeric amphiphiles were drastically altered to facilitate changes in electrostatic properties and steric bulk, inevitably causing a dramatic change in packing behavior. This results in micrometer-scale network aggregates formed in situ, thereby leading to increased retention and accumulation at tumor regions in vivo. The in situ aggregation and accumulation processes were monitored by Förster resonance energy transfer (FRET) for

over 2 days, showing an increased fluorescence intensity signal on the second day, thus demonstrating its ability as a potential imaging contrast agent with prolonged retention within tumor tissues (Figure 3b). Furthermore, it was also noteworthy that the PPAs showed negligible toxicity toward the tumors due to no difference in tumor size throughout the observation period for any of the tested subjects. Their work has validated the merits of in situ enzyme-mediated reconstruction of nanomaterials for enhanced imaging applications due to increased retention and accumulation within tumors. Subsequently, the group further adapted the design and prepared similar PPAs end-labeled with Alexa Fluor 647 as probes for whole mouse imaging.<sup>72</sup> The presence of retained material after enzyme activation was visualized via whole animal imaging in vivo following an intratumoral injection into xenograft tumors. Fluorescent aggregates were observed in targeted tumor tissues within an hour and were retained for at least a week via whole animal near-infrared (NIR) fluorescence imaging (Figure 3c), whereas control nanoparticles were cleared from tumor tissues within an hour (Figure 3d). Likewise, the material was retained for extended periods of time due to an MMP-responsive accumulation process in which the nanoparticles are transformed from spherical micelles into micrometer-scale aggregates, thus entrapping them within the tumor for a prolonged period of time.

Furin is a trans-Golgi protease which plays crucial roles in several diseases such as anthrax, Alzheimer's disease, Ebola fever, and cancer.<sup>73,74</sup> The proteolytic enzyme has been reported to be overexpressed in many different cancers such as glioblastomas, squamous-cell carcinomas of the head and neck, and nonsmall-cell lung carcinomas,<sup>75</sup> in which it preferentially cleaves the peptide substrate Arg-X-Lys/Arg-Arg, where X is any amino acid.<sup>76</sup> Inspired by the characteristics of this enzyme, Rao and co-workers reported the controlled assembly of nanostructures in living cells by virtue of a biocompatible condensation reaction.<sup>22</sup> The self-assembly is triggered by furin/caspase proteolytic cleavage, disulfide reduction, or/and pH change to reveal the 1,2-aminothiol group, at which an intermolecular condensation reaction would occur with 2-cyanobenzothiazole (CBT) from another molecule. The resulting condensation products and assembled nanostructures vary in size and morphology depending on how the condensation products were generated and the chemical structure of the monomers. Subcellular localizations of the different condensation products were also revealed through direct imaging methods in vitro, demonstrating feasibility in controlled and localized self-assembly within cells. As such, due to the aberrant overexpression of various proteases in many different types of cancers, the ability to activate the condensation process through specific upregulated proteolytic activity is particularly attractive.<sup>77–81</sup> Liang and co-workers have intuitively adapted this reaction strategy and attached various imaging agents to the monomer, leading to selective condensation, self-assembly, and accumulation of imaging agents in specific protease-overexpressed tumor cells. For instance, they first proposed a molecular design for caspase-3-mediated condensation and assembly of biotinylated nanoparticles. The reported nanoparticles were able to capture fluorescein isothiocyanate (FITC) labeled streptavidin on its surface for an enhanced "turn on" fluorescence signal<sup>82</sup> that was sensitive enough to even detect caspase-3 activity at low concentrations. Subsequently, the group went on to systematically develop magnetic resonance imaging (MRI)<sup>83</sup> (Figure

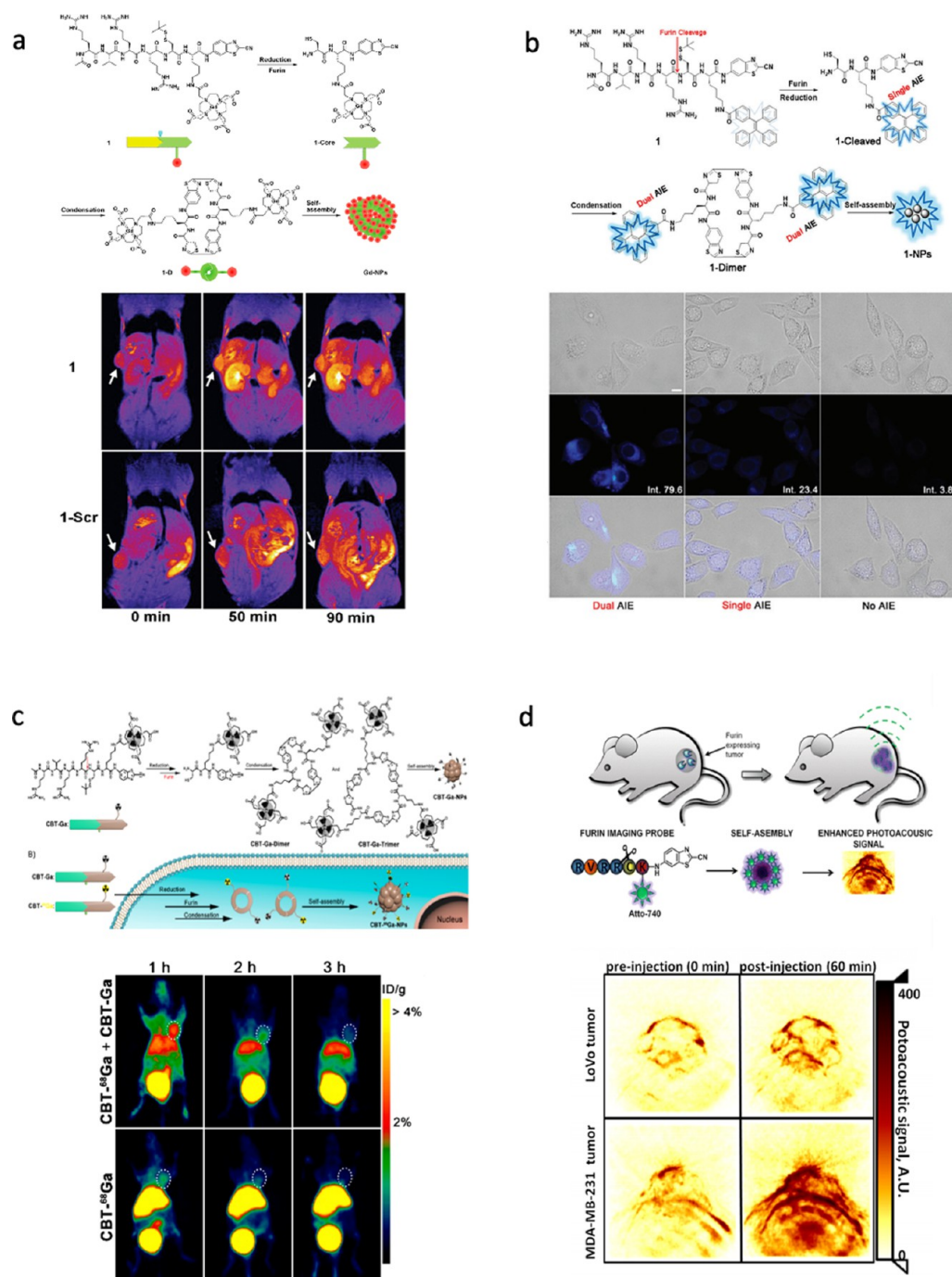


**Figure 4.** (a) Schematic illustration of a furin-controlled condensation and self-assembly of Gd-NPs with representative coronal MR images of mice with subcutaneously xenografted tumors. Reproduced with permission from ref 83. Copyright 2013 Springer Nature. (b) Schematic illustration of furin-controlled dual AIE for enhanced fluorescence sensing of furin activity with representative fluorescence imaging data in cells. Reproduced with permission from ref 84. Copyright 2017 Royal Society Chemistry. (c) Schematic illustration of furin-guided Ga nanoparticles formation and representative whole body coronal microPET images of tumor-bearing mice at different time points upon different treatments. Reproduced with permission from ref 85. Copyright 2019 American Chemical Society. (d) Schematic illustration of a furin-controlled condensation and subsequent self-assembly to generate photoacoustic contrast with representative photoacoustic images of mice tumors. Reproduced with permission from ref 87. Copyright 2013 American Chemical Society.

4a), dual AIE<sup>84</sup> (Figure 4b), and radioactive<sup>85,86</sup> (Figure 4c) probes which are able to undergo furin-controlled condensation to self-assemble into nanoparticles in tumor cells for enhanced MR contrast within tumors, improved fluorescence detection of furin activity in cells, and micropositron emission tomography (microPET) imaging of tumors in nude mice, respectively. Gambhir and co-workers have also expanded the

versatility of this enzyme-responsive bi-orthogonal condensation reaction to enhance photoacoustic imaging in vivo, reporting furin and furin-like activity in cells and tumor mice models<sup>87</sup> (Figure 4d). In addition, Liang and co-workers have also developed MRI contrast agents sensitive toward  $\gamma$ -glutamyltranspeptidase<sup>88</sup> and legumain<sup>89</sup> by utilizing the versatile condensation reaction as well.

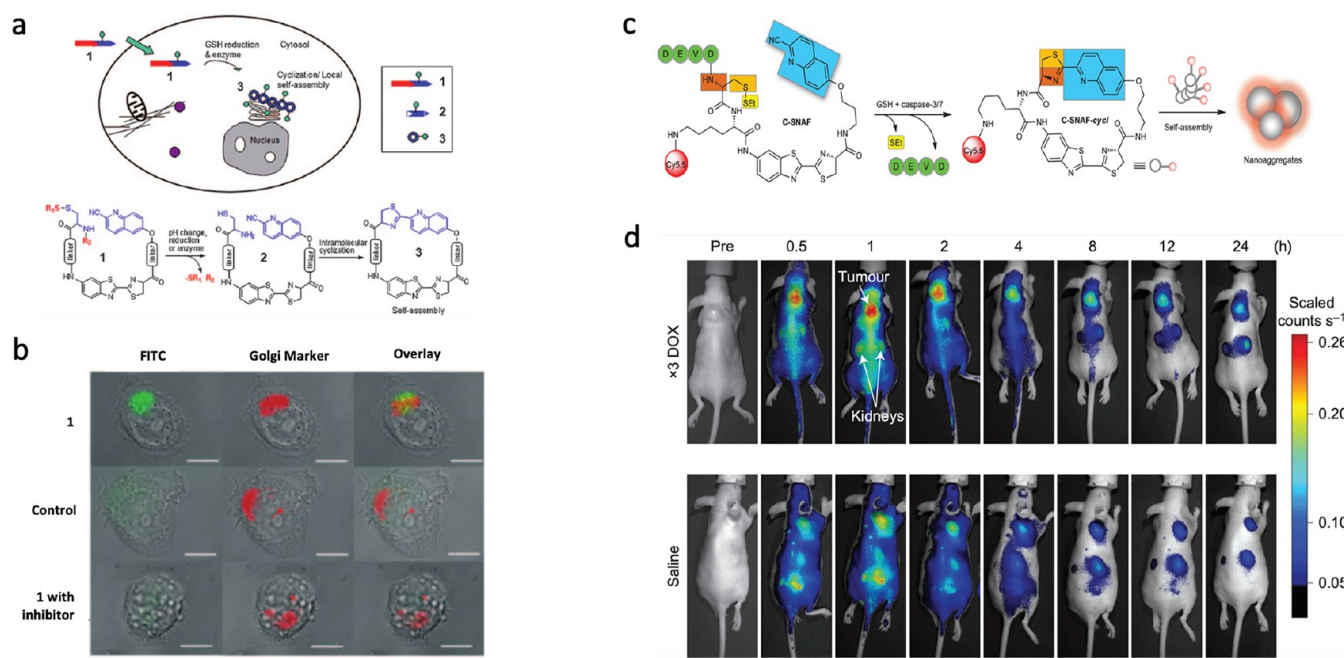


**Figure 5.** (a) Schematic illustration of enzyme-controlled macrocyclization reaction in cells. (b) Fluorescence imaging of furin-triggered localized macrocyclization in live cells. Panels a and b reproduced with permission from ref 23. Copyright 2011 Wiley-VCH. (c) Illustration of the proposed caspase-3/7 and reduction-controlled bi-orthogonal intramolecular cyclization reaction, followed by self-assembly into nanoaggregates in situ. (d) Longitudinal fluorescence imaging of doxorubicin-treated (top) and saline-treated (bottom) tumor-bearing mice over 24 h. Panels c and d reproduced with permission from ref 90. Copyright 2014 Springer Nature.

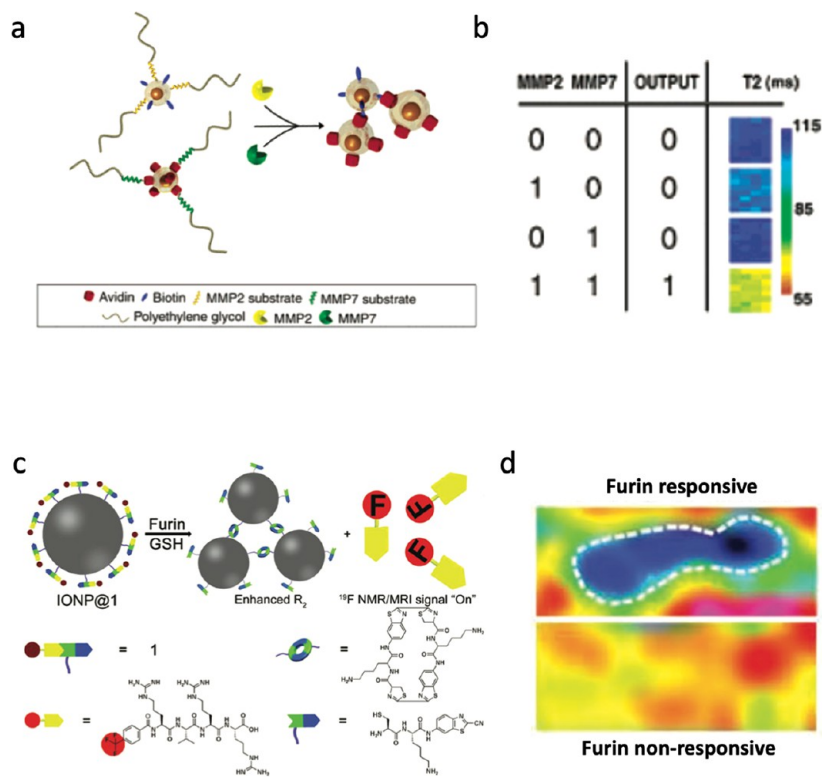


**Figure 6.** (a) Schematic representation of logical nanoparticle sensors. (b) MRI visualization of logical function. Panels a and b reproduced with permission from ref 94. Copyright 2007 American Chemical Society. (c) Schematic illustration of intracellular furin-mediated formation of nanoparticle aggregates. (d)  $^1\text{H}$  MRI of tumor in tumor-bearing zebrafish. Panels c and d reproduced with permission from ref 95. Copyright 2019 Wiley-VCH.

Thereafter, Rao and co-workers also developed an intramolecular macrocyclization strategy to image local protease

activity intracellularly<sup>23</sup> (Figure 5a). Furin proteolytic cleavage and glutathione reduction were employed to reveal the 1,2-

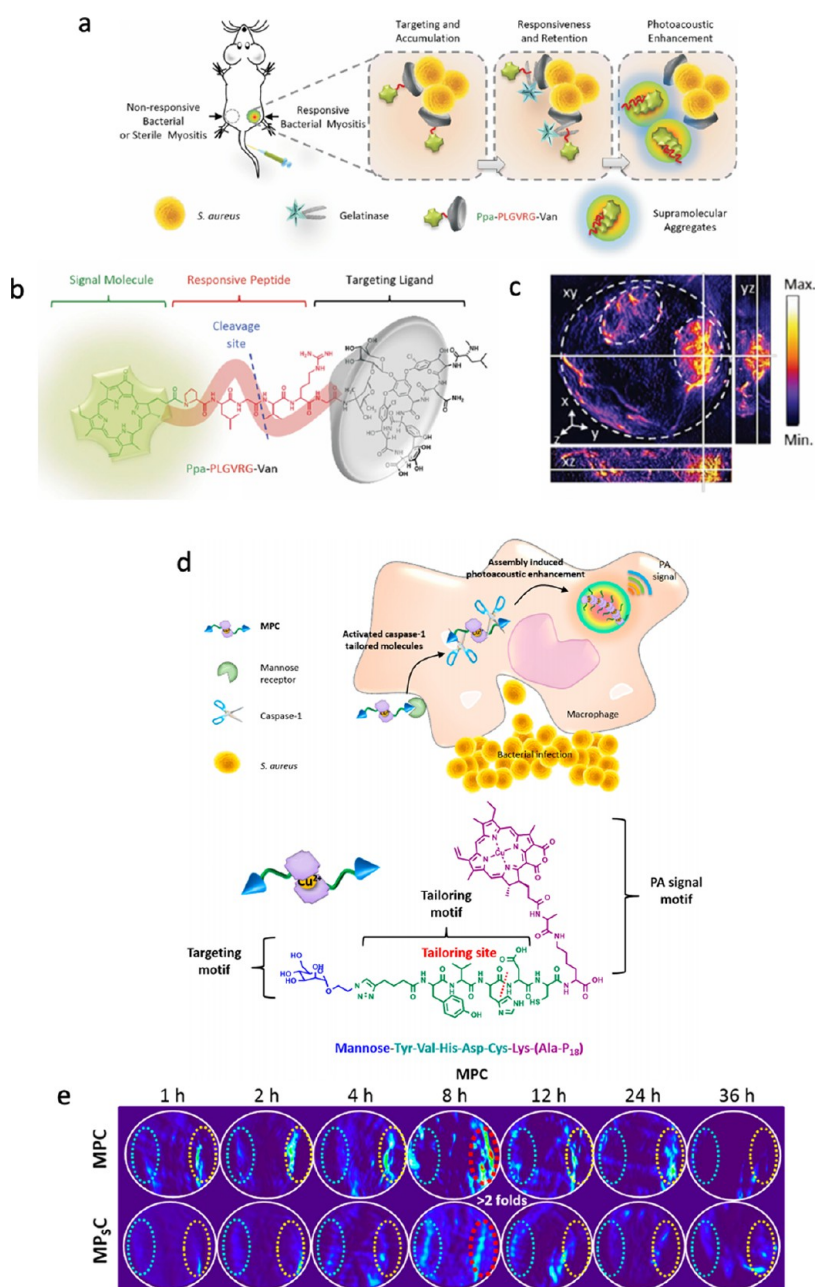


**Figure 7.** (a) Illustration of bacterial infection imaging based on an in vivo aggregation strategy. (b) Chemical structure of Ppa-PLGVRG-Van. (c) 3D reconstruction of an infected site 24 h after intravenous injection of Ppa-PLGVRG-Van. Panels a–c reproduced with permission from ref 99. Copyright 2016 Wiley-VCH. (d) Schematic representation of macrophage chemotaxis-instructed *S. aureus* infection detection in vivo and the molecular component of the probe (MPC). (e) PA images of intracellular infection in vivo over 36 h after intravenous administration of MPC and control probe. Panels d and e reproduced with permission from ref 101. Copyright 2018 American Chemical Society.

aminothiol group, at which an intramolecular condensation would take place with 2-cyano-6-hydroxyquinoline (CHQ) from the same molecule, yielding amphiphilic products that self-assemble into fluorescent nanoparticles intracellularly at sites with high furin activity (Figure 5b). In comparison with the bimolecular condensation strategy reported previously, the merit lies with added leverage of the CHQ moiety not being subjected to endogenous competition with cysteine. Furthermore, the condensation reaction is also kinetically faster and not concentration-dependent because it takes place intramolecularly. Improved correlation between aggregation sites and location of high enzymatic activity can be achieved as the enzymatic activity is now the rate-limiting step in the

formation of the aggregated macrocycles. Subsequently, many have adapted this reaction strategy and developed a series of peptide-based nanoprobe responsive toward caspases in order to study cellular apoptosis. For instance, Rao and co-workers first reported caspase-3/-7-triggered bi-orthogonal macrocyclization to form nanoaggregates allowing for the effective monitoring of chemotherapy response in vivo<sup>90</sup> (Figure 5c). Upon enzymatic cleavage and intramolecular macrocyclization, the rigid and hydrophobic residues successfully aggregated in situ, allowing for in vivo tumor responses to be detected serially throughout the entire course of chemotherapy (Figure 5d) due to strong correlation between changes in tumor size and degree of observed fluorescence. Along with its non-

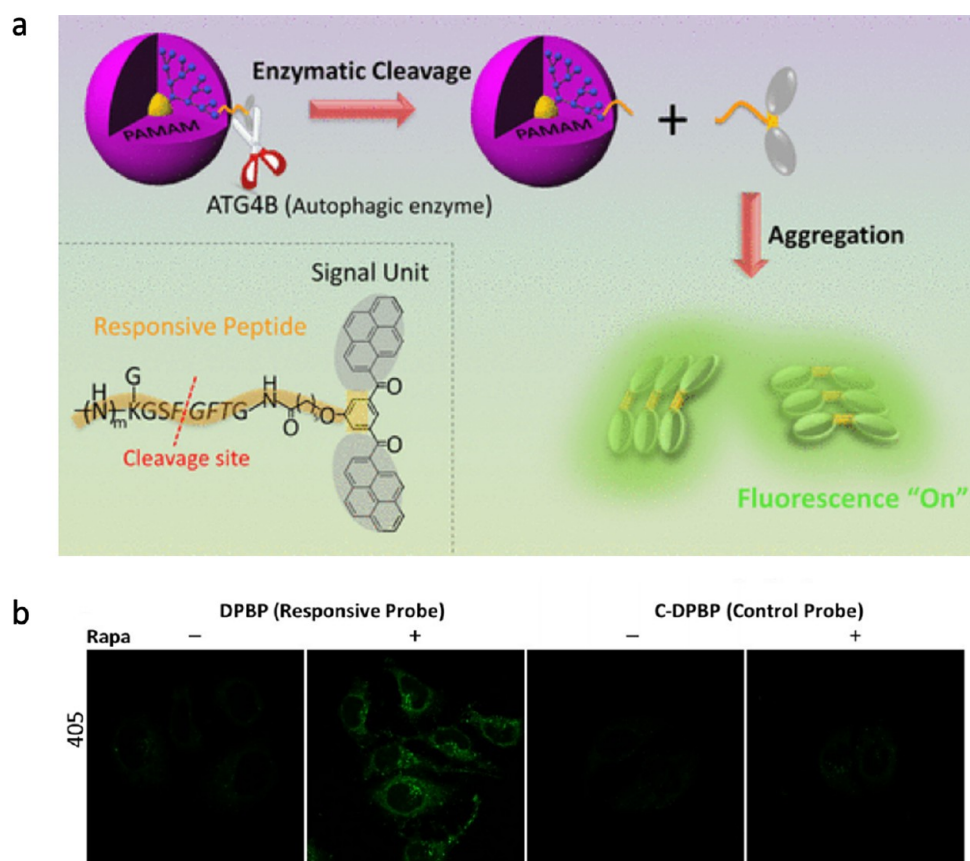


**Figure 8.** (a) Schematic illustration of DPBP as a probe for autophagy detection. (b) CLSM images of normal and autophagic (rapamycin-treated) cells treated with DPBP and C-DPBP (control probe). Panels a and b reproduced with permission from ref 108. Copyright 2017 American Chemical Society.

invasive nature, the designed probe demonstrated potential practical applications in rapid and real-time imaging of drug-induced tumor apoptosis. Shortly after, utilizing the same caspase-mediated nanoparticle self-assembly approach, caspase-3/-7 activatable gadolinium-based MRI probes were developed to study tumor apoptosis in mice<sup>91</sup> and stem cell apoptosis in arthritic joints.<sup>92</sup> Ye and co-workers have also expanded the versatility of this proteolytic enzyme mediated intramolecular macrocyclization reaction to enhance the performance of photoacoustic imaging.<sup>93</sup>

Other than biocompatible condensation and intracellular macrocyclization reaction strategies for controlled assembly of nanostructures in living cells, enzyme-activated self-assemblies have also been further adapted for intracellular aggregation of nanoparticles surface conjugated with responsive peptide substrates. Bhatia and co-workers first reported the design and synthesis of nanoparticles that perform Boolean logic operations using two proteolytic inputs (MMP-2/-7) associated with unique aspects of tumorigenesis (Figure 6a).<sup>94</sup> Two different kinds of super-paramagnetic  $Fe_3O_4$  nanoparticles were designed, the first comprising a tethered biotin ligand and the other its neutravidin receptor. Subsequent conjugation of peptide-polyethylene glycol (PEG) via MMP-2/-7 substrates restricted coalescence of the nanoparticles to only occur in the presence of the enzymes. The enzyme-mediated self-assembly of initially dispersed super-paramagnetic  $Fe_3O_4$  nanoparticles amplified the  $T_2$  relaxation rate of the hydrogen protons (Figure 6b), enabling remote, MRI-based detection of logical operations, showing potential applications in monitoring

complex disease signatures such as cancer. Much later on, Liang and co-workers intuitively made use of furin- (Figure 6c)<sup>95</sup> and caspase-3/-7-responsive<sup>96</sup> biocompatible condensation reaction strategies to similarly activate the aggregation of  $Fe_3O_4$  nanoparticles for enhanced  $T_2$  MR imaging of tumors (Figure 6d) and tumor apoptosis as well. Most recently, the photothermal conversion efficiency of furin-aggregated  $Fe_3O_4$  nanoparticles was also evaluated for potential image-guided photothermal therapy.<sup>97</sup>

**2.2. Detection of Bacterial Infections.** Apart from the manifestation of tumors, bacterial infections are also significant clinical diseases with high mortality rates. While traditional antibiotic treatment can effectively eliminate bacteria, its long-term widespread use has led to an evolution of resistance.<sup>54</sup> Hence, the increase in bacterial resistance<sup>98</sup> has demanded for in situ self-assembled nanomaterials to be adapted as probes for rapid and accurate detection of bacterial infections. For instance, Wang and co-workers have adapted in situ aggregation strategies for peptide-based nanoprobe to greatly enhance photoacoustic detection of bacterial infections. They first reported a peptide molecular probe that is able to differentiate sterile inflammation from bacterial infection in vivo, specifically identifying gelatinase-positive and Gram-positive bacterial species with high sensitivity<sup>99</sup> (Figure 7a). The molecular probe (Ppa-PLGVRG-Van) consists of vancomycin (Van) as a targeting ligand and pyropheophorbide- $\alpha$  (Ppa) as a signaling molecule linked together by a gelatinase-responsive peptide linker (Pro-Leu-Gly-Val-Arg-Gly) (Figure 7b). Ppa-PLGVRG-Van selectively binds to the

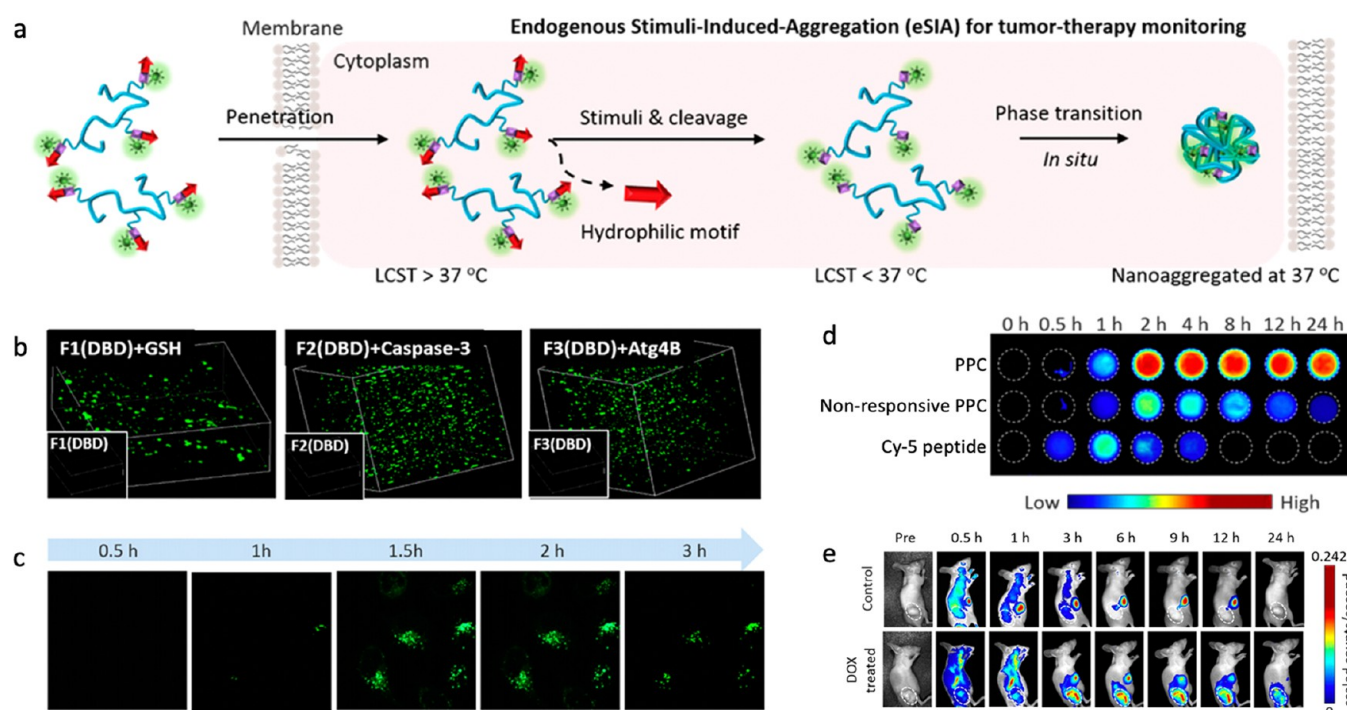


**Figure 9.** (a) Schematic representation of stimuli-instructed construction of controllable nanoaggregates for monitoring tumor therapy response. (b) Confocal images of corresponding PPCs with and without (inset images) treatment of the correlated stimuli. (c) Real-time confocal images of cells after treatment with PPCs. (d) Retention effect of PPCs in viable cells. (e) Longitudinal fluorescence imaging of PPCs monitoring therapeutic results. Panels a–e reproduced with permission from ref 109. Copyright 2017 American Chemical Society.

cell wall of Gram-positive bacteria, while the overexpression of gelatinase then selectively cleaves the peptide linker, releasing residues with enhanced hydrophobicity that aggregate and subsequently self-assemble in the form of twisted fibers. Bacterial infections were reported to be accurately detected real-time and non-invasively due to the increased efficiency in heat conversion and amplification of the photoacoustic signal (Figure 7c). Intriguingly, photoacoustic signals for *Staphylococcus epidermidis* (*S. epidermidis*; Gram-positive strain) and *Proteus vulgaris* (*P. vulgaris*; gelatinase releasing strain) were around two times brighter than the control, whereas the enhanced photoacoustic signal observed for *S. aureus* (Gram-positive and gelatinase releasing strain) was more than three times stronger. After successful implementation of their first chlorophyll-peptide system, the group further strived to quantitatively detect bacterial infections real-time.<sup>100</sup> They proposed caspase-1 (bacterial infection precaution protein) activated substrate molecules (P18-YVHDC-TAT) and monitored the dynamic equilibrium of binary states through ratiometric photoacoustic signals. Enzymatic activities were successfully quantified without cell lysis due to strong correlation between the observed signal and aggregation tendency, paving way for quantitative and non-invasive detection of bacterial infections in vivo. Subsequently, Wang and co-workers designed another chlorophyll peptide-based photoacoustic agent with the ability to detect intracellular *S. aureus* infections<sup>101</sup> (Figure 7d). The peptide-based photoacoustic agent, mannose-Tyr-Val-His-Asp-Cys-Lys-(Ala-P18) (MPC), is comprised of three parts, an active targeting ligand (mannose), a tailoring motif sensitive toward caspase-1 enzymatic cleavage, and a photoacoustic signaling motif. Upon recognition and internalization by infected macrophages, activated caspase-1 cleaves the peptide substrate and detaches

its photoacoustic signaling motif. The residues accumulate and assemble to form J-type aggregates capable of aggregation-induced retention effect, significantly enhancing the infected regions by over 2.6-fold (Figure 7e). The MPC showed improved specificity and sensitivity in the bio-imaging of bacteria, enabling the in vivo detection of early stage bacterial infections. In addition, Wang and co-workers have most recently developed gold nanoparticles modified with functional peptides as photoacoustic contrast agent for detection of bacterial infections in vivo.<sup>102</sup> Nanoparticles (AuNPs@P1) were specifically tailored with surface peptides responsive toward bacterial-overexpressed collagenase IV to confer in situ aggregation properties upon proteolytic activation, resulting in increased nanoparticle accumulation at infected sites along with active targeting. The dynamic aggregation of AuNPs@P1 along with local surface plasmon resonance (LPSR) effect showed dramatically enhanced photoacoustic signals, potentially providing an alternative approach toward the early detection of bacterial infections in vivo.

**2.3. Other Imaging Applications.** Autophagy is an essential metabolic process dependent on the lysosome to remove dysfunctional organelles and damaged proteins for degradation.<sup>103</sup> It is often associated with numerous mammalian pathologies<sup>104,105</sup> including infections,<sup>106</sup> neurodegenerative disorders,<sup>55</sup> and aging.<sup>107</sup> As such, the study of autophagic levels and their function during therapeutic processes would be vital in providing useful information for improved therapeutic potential. Wang and co-workers reported an effective responsive probe capable of monitoring autophagy in living cells real-time<sup>108</sup> (Figure 8a). The probe (DPBP) consists of a bulky dendrimer carrier linked with bis(pyrene) signaling molecules on the surface via autophagy-specific enzyme (Atg4B) responsive peptide linkers. Observed to be

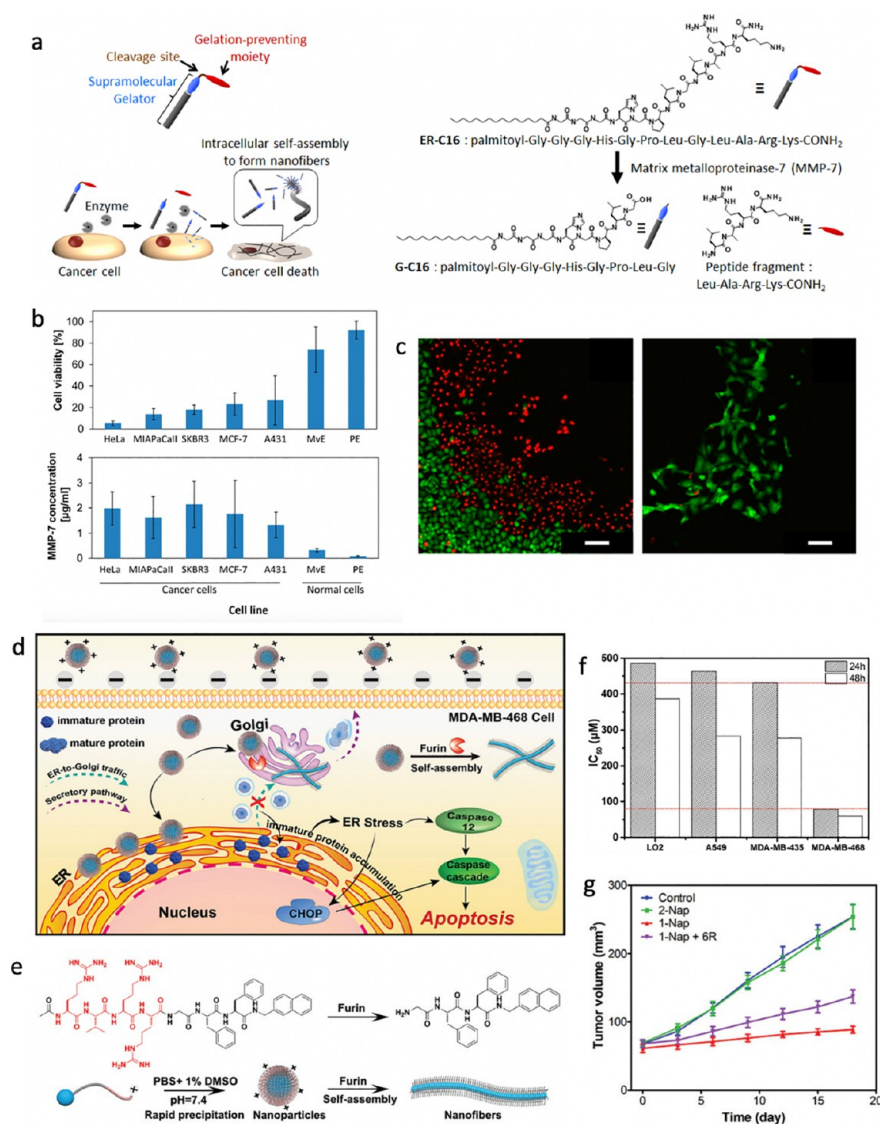


**Figure 10.** (a) Schematic illustration of cancer cell death induced by molecular self-assembly of an enzyme-responsive supramolecular gelator and molecular structure of ER-C16. (b) Viability assays of cancer cells and normal human cells after incubation with ER-C16 and MMP-7 concentration in the culture media after culturing the cells. PE represents primary human pancreatic epithelial cells. (c) Live/dead assays of HeLa cells (left) and MvE cells (right) using CLSM and a coculture system. Panels a–c reproduced with permission from ref 111. Copyright 2015 American Chemical Society. (d) Schematic illustration of the furin-instructed self-assembly of 1-Nap for cancer cell inhibition. (e) Chemical structure and schematic illustration of the conversion of 1-Nap into nanoparticles via a rapid precipitation process and furin-instructed conversion of the nanoparticles into nanofibers. (f) IC<sub>50</sub> values of 1-Nap against different cell lines. (g) In vivo anticancer efficacy of the different compounds. Panels d–g reproduced with permission from ref 117. Copyright 2020 Royal Society of Chemistry.

quenched in normal cells, the fluorescence property of DPBP is activated only upon autophagic activation which releases the bis(pyrene) signaling moiety. Self-assembling properties of the residues allowed a 30-fold dramatically enhanced fluorescence for autophagic levels to be quantitatively evaluated. As shown by confocal laser scanning microscopy (CLSM) data, rapamycin-treated (autophagy-induced) cells were observed with intense green fluorescence by DPBP, whereas no obvious signal was obtained from cells incubated with a control containing an unresponsive peptide sequence (Figure 8b). This work has demonstrated the merits of in situ enzyme-mediated intracellular self-assembly in providing a fast and effective method to quantitatively monitor autophagic levels real-time in living systems, potentially becoming a useful tool for future autophagy-related studies.

Alternatively, autophagy and other physiological changes were also monitored via a general endogenous stimuli-induced aggregation (eSIA) strategy, in which functional nanoaggregates were constructed in situ due to the isothermal phase transition property of thermosensitive polymer-peptide conjugates (PPCs)<sup>109</sup> (Figure 9a). The designed PPCs mainly comprise three parts, a thermosensitive polymer backbone (PNIPAAm), a signal-molecule label, and a grafted hydrophilic peptide side chain with endogenous stimuli-cleavable motifs. Initially, the PPCs exist in extended states with lower critical solution temperatures above 37 °C. Upon enzymatic cleavage of the hydrophilic peptide, the residues with decreased lower critical solution temperatures (less than 37 °C) spontaneously self-assemble to form uniform spherical nanoaggregates (600–700 nm) intracellularly. Subsequent labeling of the PPCs with fluorescent molecules allowed for signal correlation with three

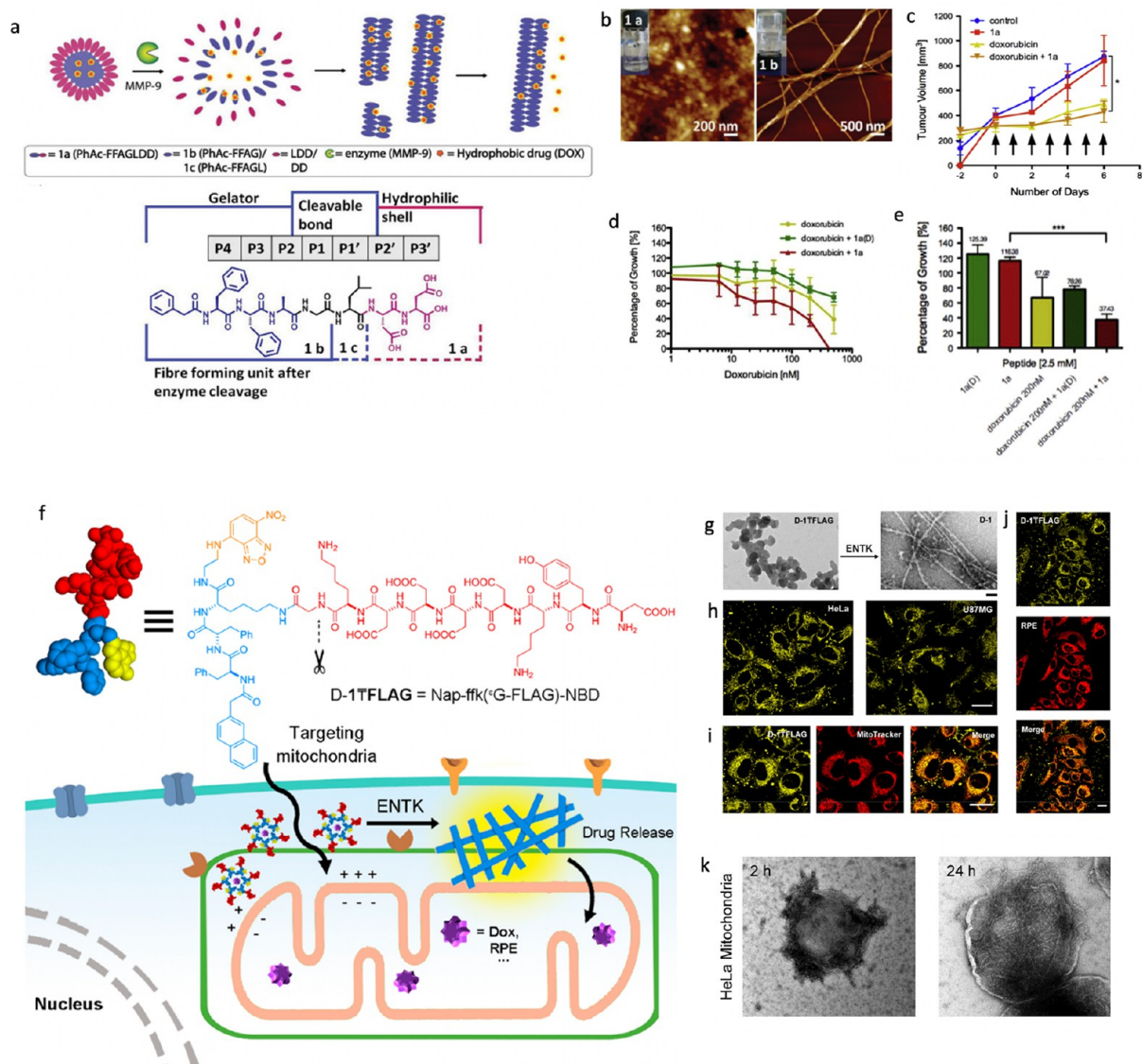


**Figure 11.** (a) Schematic representation of micelle to fiber transition induced by MMP-9 cleavage for prolonged drug release and chemical structure of the biocatalytic gelation system and its components. (b) Atomic force microscopy (AFM) images showing micellar aggregate to fiber transformation. Panels a and b reproduced with permission from ref 118. Copyright 2015 Royal Society of Chemistry. (c) In vivo tumor progression of treated tumors. (d) Effect of MMP-9-cleavable peptides and doxorubicin on proliferation of cells in vitro and (e) corresponding MTT assay data. Panels c–e reproduced with permission from ref 119. Copyright 2016 Elsevier. (f) Structure of representative branched peptide and ENTK cleaving the branch to convert micelles to nanofibers on mitochondria. (g) TEM images of micelle to fiber transformation after adding ENTK. (h) Fluorescent images of HeLa and U87MG cells incubated with branched peptide for 2 h. (i) Fluorescence images of branched peptide and MitoTracker in HeLa cells. (j) HeLa cells treated with RPE and branched peptide for 2 h. (k) TEM images of mitochondria isolated from HeLa cells after being incubated with branched peptide for 2 and 24 h. Panels f–k reproduced with permission from ref 120. Copyright 2018 American Chemical Society.

different endogenous stimuli of interest: Atg4B for autophagy, glutathione (GSH) reduction for antioxidant defense, and caspase-3 for apoptosis (Figure 9b). Long-term fluorescence spectroscopic recording of the aggregation process revealed that the nanoaggregates exhibited enhanced retention effect in cells due to stimuli-induced aggregation (Figure 9c). Furthermore, compared to nonresponsive PPCs and dye-labeled peptides, the responsive PPCs also showed significantly brighter signals from 2 h postincubation for up to 24 h (Figure 9d), allowing for quantification and specific identification of the corresponding endogenous factor. This generic strategy is expected to facilitate high-performance dynamic monitoring of therapeutic progresses in vivo (Figure 9e).

### 3. PROTEASE-ACTIVATED SELF-ASSEMBLIES FOR THERAPY

Apart from accumulation of imaging agents for early disease diagnostics, active retention of therapeutic material at the targeted diseased area is also crucial for effective treatment subsequently. Although some therapeutic small molecules have been developed to effectively target diseased areas, they are often prematurely excreted, thus reducing their bio-availability for an effective therapeutic effect.<sup>110</sup> To solve this problem, an added ability to assemble into larger nanostructures in situ can help retain therapeutic agents at target sites for prolonged periods of time. Due to differing microenvironments between infected and normal tissues, developments in specific

construction of assemblies in infected areas have demonstrated promising therapeutic applications such as in having antitumor and antibacterial properties, acting as drug carriers, aiding in photosensitizer delivery and even wound recovery.

**3.1. Self-Assemblies with Anti-tumor Effect.** The formation of assemblies with antitumor properties is an interesting strategy that affects tumor cells directly through intracellular self-assembly of peptide derivatives. This selectively causes stress to the affected organelles and specifically leads to the death of tumor cells eventually. Maruyama and co-workers first reported an MMP-7-responsive supramolecular gelator<sup>111</sup> which undergoes intracellular self-assembly to induce the death of cancer cells (Figure 10a). The designed supramolecular gelator precursor (ER-C16) comprises four distinct components, a 16-carbon alkyl chain which contributes hydrophobic interactions that can enhance the self-assembly in aqueous solution, an amphiphilic tetrapeptide segment that is able to act as both hydrogen bond acceptor and donor and is thus a major building block, a peptide sequence cleavable by cancer-related overexpressed MMP-7 that can induce the self-assembly giving rise to gelation, and last a cationic peptide sequence which prevents premature formation of nanofibers before enzymatic hydrolysis. Cancer cells secreting exorbitant quantities of MMP-7 transform the precursor into the supramolecular gelator before they are taken up by the cells. Once inside the cells, the supramolecular gelator molecules self-assemble into nanofibers which exerted vital stress on the affected cells, critically impairing their cellular function which led to an inevitable cell death. The different amounts of MMP-7 secreted specifically by cancer cells were found to be proportional to the cytotoxicities observed. Furthermore, the gelator precursor was reported to show low cytotoxicity toward normal cells but prominent cytotoxicity toward five dissimilar cancer cell lines (Figure 10b). The exposure of the precursor to a coculture of normal and cancer cells confirmed that the cytotoxicity was selective toward cancer cells (Figure 10c). Since the cytotoxic mechanism is unique, cancer cells are unlikely to develop resistance to this technique in comparison to molecularly targeted treatment and conventional cytotoxic chemotherapy, hence holding great potential for novel therapeutic applications in which molecular self-assembly is the mechanism for observed cytotoxicity.

Proteostasis is a vital biological process in order to maintain cellular survival. Its distortion results in the buildup of endoplasmic reticulum (ER) stress, eventually initiating cellular apoptosis.<sup>112,113</sup> Neurodegenerative diseases can be caused by severe ER stress-mediated apoptosis, therefore highly anticipated as a new therapeutic target for cancer therapy.<sup>114–116</sup> Inspired by this phenomenon, Ou and co-workers have utilized furin-controlled self-assembly of nanofibers in situ to actuate ER stress-mediated apoptosis for potential cancer therapy<sup>117</sup> (Figure 10d). They designed a small molecule (1-Nap) comprising a self-assembling peptide moiety (GFF-Nap) directly conjugated to a positively charged tetrapeptide furin-cleavable sequence (RVRR). This not only endows the molecule with the ability to easily internalize into cells but also enables its attachment to membranous organelles such as the Golgi body and ER. The designed small molecules can self-assemble *ex situ* into spherical nanoparticles (69.9–149.1 nm) under stirring with the hydrophilic peptide segment as the outer layer and aromatic peptide residues packed inside with the naphthyl group. Upon enzymatic cleavage in furin-

overexpressed tumor environments, the initial spherical 1-Nap nanoparticles transformed and self-assembled into long filamentous 1-Nap nanofibers (8.9–13.4 nm) (Figure 10e). Further experimental data have confirmed that the self-assembling ability of 1-Nap instructed by furin is indispensable in actuating ER stress and subsequent activation of tumor apoptosis despite its ER-targeting interactions. As such, the group reasonably hypothesized that the transport of proteins from ER to Golgi required for proteostasis and homeostasis was cut off by the fibrous assemblies near the Golgi complex. This subsequently activates the ER stress-mediated apoptosis to attain antitumor and cancer suppression effects selectively in furin-overexpressed cell lines (Figure 10f) and solid tumors in vivo (Figure 10g). Their work has provided the possibility for new developments in cancer therapeutics by virtue of targeted disruptions to cellular proteostasis through molecular self-assembly.

**3.2. Self-Assemblies for Drug Delivery.** Self-assemblies can also act as nanocarriers for drugs to target sites, facilitating in their effective transport and sustained release for enhanced therapeutic effects. Uljin and co-workers first reported the termination of tumor growth by MMP-9-activated construction of doxorubicin-loaded nanofibrous depots.<sup>118,119</sup> The group designed peptide amphiphiles that exist as spherical micelle aggregates initially (Figure 11a). Upon activation of MMP-9, the amphiphiles subsequently undergo an *in situ* enzyme-triggered transformation to form filamentous fibers intracellularly (Figure 11b). In addition to the possible morphological change, the micelles were also reported as potential mobile drug carriers due to their ability in effectively encapsulating doxorubicin for subsequent controlled release. Taking advantage of aberrant MMP-9 overexpression in various cancers, these mobile drug carriers have been specially engineered to transport the payload to tumors specifically by assembling into localized fiber depots. Sustained drug releases for prolonged periods were successfully observed as a result of the intrinsic biodegradability of the peptide carriers and its partial drug entrapment. Further experiments conducted with xenograft tumor models revealed the stunt in tumor growth caused by administration of the doxorubicin-loaded peptide amphiphiles (Figure 11c,d). Additionally, the peptide amphiphiles were reported with negligible toxicity toward cells (Figure 11e), therefore very suitable as potential *in vivo* carriers of doxorubicin unlike previously reported peptide conjugates used for drug delivery. Furthermore, in contrast to available combination therapies in which the sole peptide component itself already displays toxicity, the nontoxic nature of the reported carrier would greatly improve the therapeutic efficacy of the anticancer drug. As such, the group has successfully assimilated guided therapy with the pathological hallmark of metastasis, in which a negative prognostic indicator was reversed to trigger a treatment response instead. It is no doubt that their work presented new perspectives into the design of novel enzyme-activated carriers for drug delivery with potential practical applications in cancer therapy.

Recently, Xu and co-workers reported using enzyme-activated self-assembly to target the delivery of cargos to the mitochondria, illustrating an alternative to target subcellular organelles for biomedical applications<sup>120</sup> (Figure 11f). The reported branched peptide molecule consists of the well-known protein FLAG-tag as the substrate for enzyme recognition and cleavage, conjugated via a glycine linker to a self-assembling peptide sequence with improved fluorescence

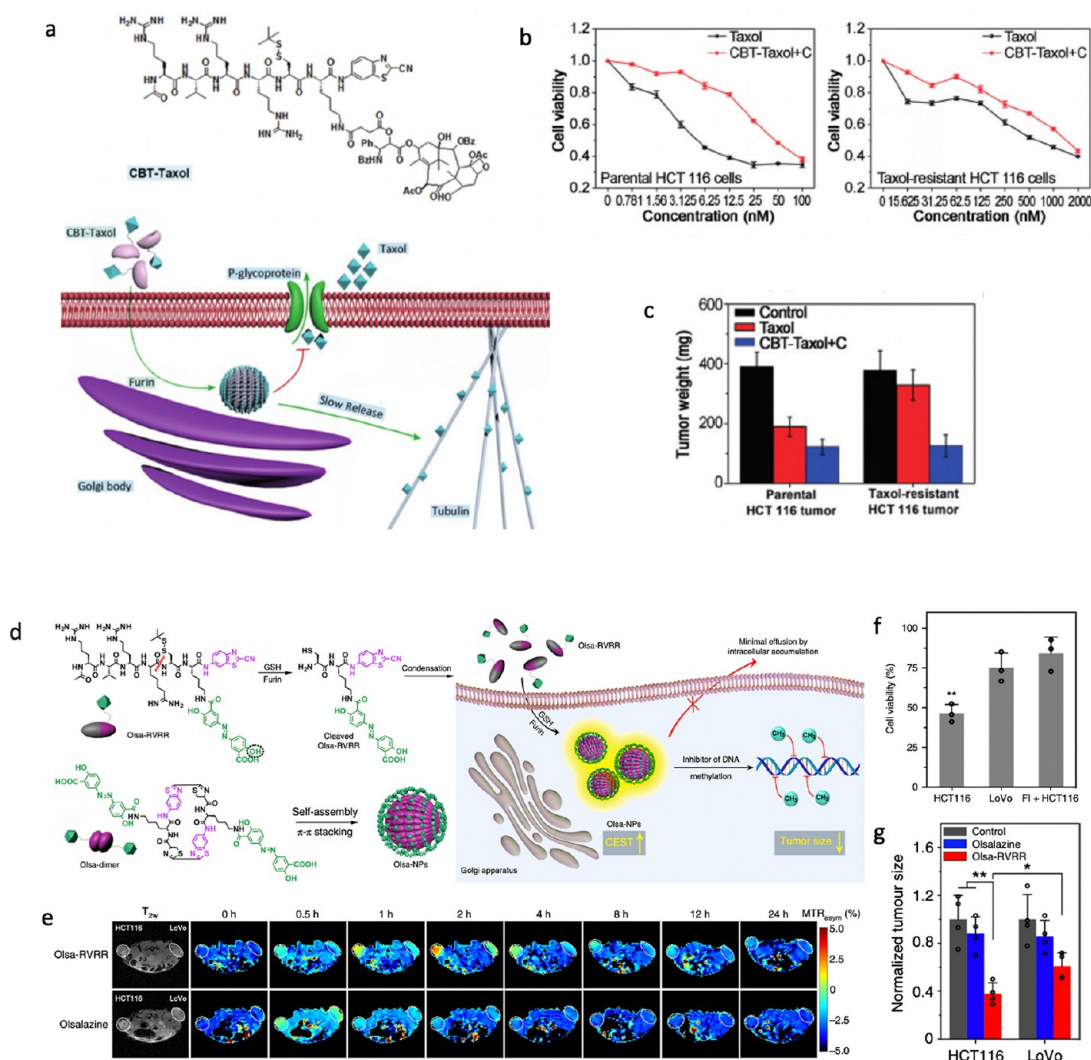


**Figure 12.** (a) Chemical structures of CBT-Taxol and schematic illustration of intracellular furin-controlled self-assembly of Taxol-NPs for anti-MDR. (b) Cell viability study of parental HCT 116 cells and Taxol-resistant HCT 116 cells on treatment with Taxol or CBT-Taxol. (c) Tumor weight of nude mice treated with control vehicle, Taxol, and CBT-Taxol co-injected with CBT precursor. Panels a–c reproduced with permission from ref 121. Copyright 2015 Wiley-VCH. (d) Schematic illustration for the formation of Olsa-NPs by furin-mediated intracellular reduction and condensation of Olsa-RVRR for enhanced CEST signal and tumor treatment efficacy. (e) MRI of tumor-bearing mice after intravenous injection of Olsa-RVRR or Olsa. (f) Cell viabilities of HCT116, LoVo, and furin inhibitor (FI) pretreated HCT116 cells incubated with Olsa-RVRR. (g) Relative tumor sizes at day 33. Panels d–g reproduced with permission from ref 122. Copyright 2019 Springer Nature.

upon self-assembly due to incorporation of a nitrobenzoxadiazolyl ethylenediamino moiety, affording micelle-forming precursors. Upon uptake by the cells, intracellular enterokinase (ENTK) cleaves the hydrophilic FLAG motif (DDDDK), transforming the micelles into nanofibers (Figure 11g) which were localized mainly at the mitochondria of tumor cells (Figure 11h,i). Micelles made up of the precursor molecules were reported with the ability to deliver cargos such as red phycoerythrin (RPE) and doxorubicin (Dox) into cells, mainly to the mitochondria in 2 h (Figure 11j). Cells treated for 2 and 24 h were observed with nanoparticles and nanofibers surrounding the mitochondria, whereas controls were observed with neither (Figure 11k). And as expected, mitochondria targetability similarly diminished upon ENTK proteolytic inhibition. Their work demonstrated an alternative successful mitochondrion targeting strategy based on enzyme-mediated transformation of negatively charged branched peptides. Interestingly, this is also the first reported attempt in delivering

molecular cargo specifically to the mitochondria via an enzymatic self-assembly, therefore providing new perspectives into the process of targeting subcellular organelles with innovative molecular design for biomedicine and potential future applications of protease-instructed assembly.

Alternatively, the biocompatible condensation strategy previously mentioned for regulated construction of intracellular nanostructures was subsequently adapted for therapeutic drug delivery applications.<sup>22</sup> Liang and co-workers reported a new approach in tackling multidrug resistance (MDR) via an intracellular self-assembly of nanodrugs<sup>121</sup> (Figure 12a). The reported Taxol derivative (CBT-Taxol) comprises 2-cyanobenzothiazole (CBT), disulfide-functionalized cysteine, Taxol conjugated to the lysine side chain, and positively charged tetrapeptide substrate (RVRR) for specific furin recognition and improved cellular uptake. Upon entering a furin-overexpressed tumor microenvironment, CBT-Taxol is reduced by glutathione and undergoes furin-mediated

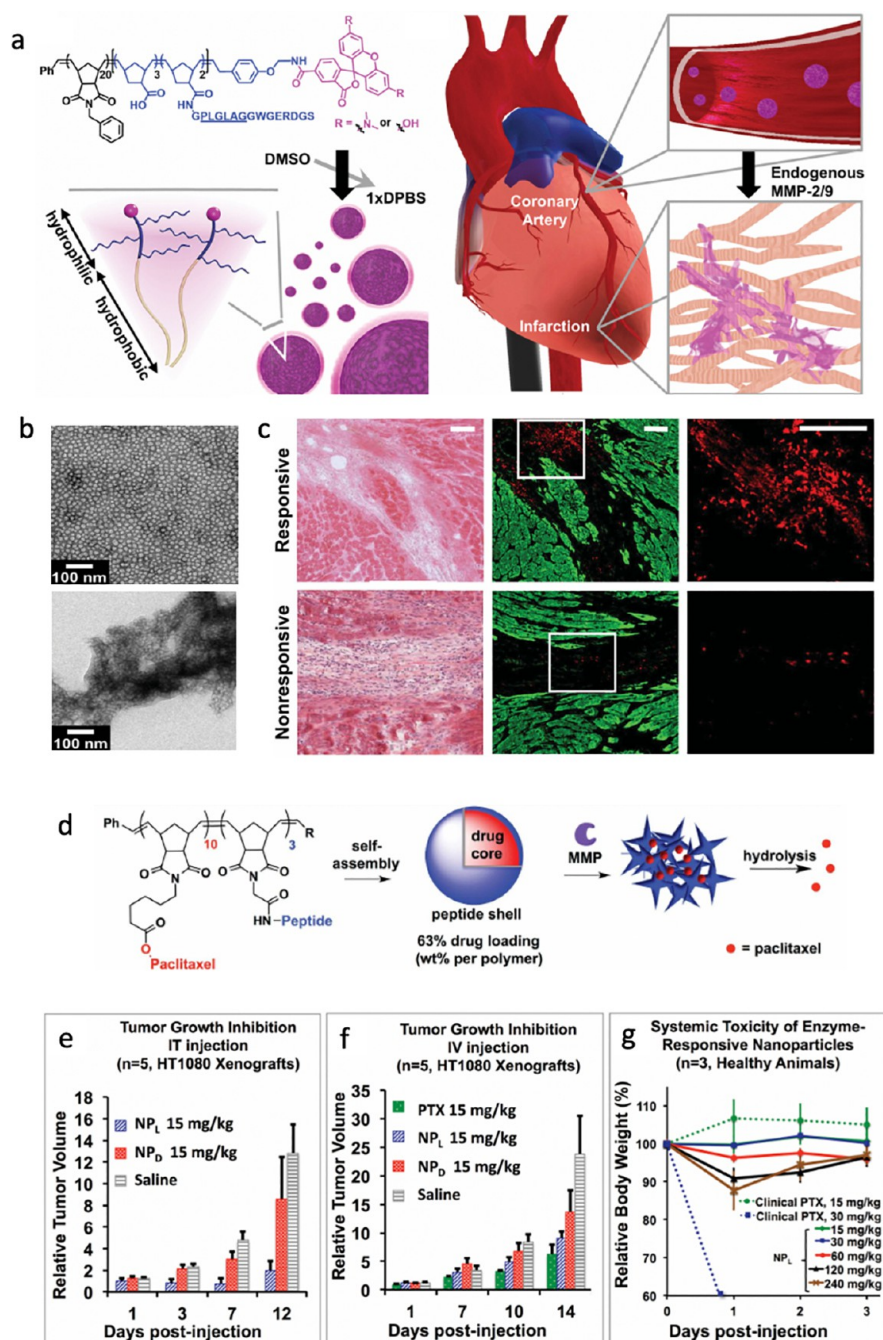


**Figure 13.** (a) Chemical structure of PPAs and schematic illustration of its self-assembly and subsequent delivery to infarct tissue through leaky acute MI vasculature and forming aggregate-like scaffold. (b) TEM images of nanoparticles (top) transformed to aggregate-like scaffold (bottom) upon activation. (c) Retention of responsive nanoparticles assessed 6 days postinjection. H&E images displaying the infarct area (left) and neighboring fluorescent sections (middle). Particles are shown in red, and myocardium is shown in green. Selected regions (white outline) were magnified to highlight particle aggregation (right). Panels a–c reproduced with permission from ref 123. Copyright 2015 Wiley-VCH. (d) Schematic illustration of nanoparticle assembly and subsequent morphology change in response to MMP. (e) Comparison of MMP-responsive nanoparticles (blue) to non-MMP-responsive nanoparticles (red) following intratumoral injection. (f) Comparison of MMP-responsive nanoparticles (blue) and non-MMP-responsive nanoparticles (red) vs clinical PTX (green) following an intravenous injection. (g) MTD of intravenous injection of MMP-responsive nanoparticles and clinically formulated PTX. Panels d–g reproduced with permission from ref 124. Copyright 2015 Wiley-VCH.

condensation to produce hydrophobic oligomers that spontaneously self-assemble into Taxol nanoparticles (Taxol-NP) at localized areas with high furin activity, especially near the Golgi bodies. Consequential to their large size and hydrophobicity, the Taxol-NPs adhere firmly onto the membrane of organelles and are thus less likely to be pumped out by P-glycoprotein.

This effectively resulted in prolonged intracellular circulation for slow and sustained therapeutic release of free Taxol to continuously bind with tubulin for a reduced MDR in cancer cells. Apart from being a furin recognition substrate, the cell-penetrating peptide (RVRR) was also reported to greatly improve the bio-availability, cellular uptake, and water

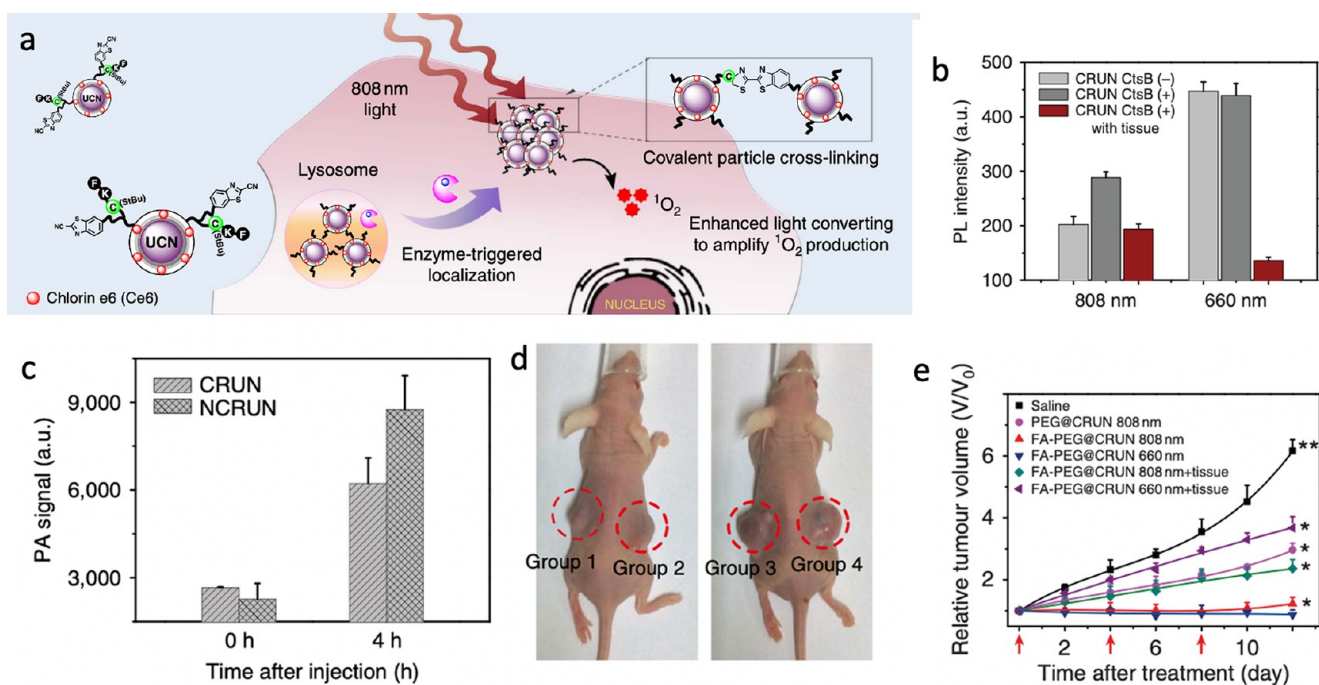


**Figure 14.** (a) Illustration of the microenvironment-sensitive strategy for covalent cross-linking of peptide-premodified UCNs in tumor areas. (b) Quantification of singlet oxygen generation before and after enzyme-triggered CRUN or covered by 2 mm thick pork tissue when exposed to 808 or 660 nm laser irradiation. (c) Photoacoustic signals in tumor region after injection of CRUN. (d) Photographs of tumor-bearing mice after 11 days of treatment with CRUN (group 1), NCRUN (group 2), CRUN without NIR light irradiation (group 3), and saline (group 4). (e) Tumor volume change as a function of time in treated groups to evaluate the effectiveness of PDT treatment in vivo. Panels a–e reproduced with permission from ref 125. Copyright 2016 Springer Nature.

solubility of Taxol. Not only did the intracellular self-assembly of Taxol-NPs prolong its circulation time, it also significantly increased the local concentration of Taxol. Biocompatibility of the entire strategy was assured throughout, starting from the choice of raw materials used for synthesis to the condensation reaction selected to assemble the Taxol-NPs. CBT-Taxol demonstrated 4.5- and 1.5-fold increased anti-MDR performances compared to Taxol in vitro (Figure 12b) and in vivo (Figure 12c), respectively. The experiments were conducted with Taxol-resistant HCT116 cancer cells and implanted tumors, with CBT-Taxol showing negligible toxicity toward the experimented cells and mice. Their results have demonstrated the potential of a new and optimized approach in overcoming tumor MDR by virtue of intracellular self-assembly of protease-labile agents into nanodrugs.

Subsequently, Bulte and co-workers also adapted the strategy for enhanced MRI and tumor therapy via furin-activated intracellular self-assembly of olsalazine nanoparticles<sup>122</sup> (Figure 12d). The group conjugated cell-penetrating peptide (RVRR) to olsalazine (Olsa), an anticancer agent. Exploiting the biocompatible condensation reaction, individual Olsa-RVRR molecules were aggregated by tumor-associated enzyme furin in situ, forming large intracellular nanoparticles. Chemical exchange saturation transfer (CEST) MRI due to the exchangeability of Olsa hydroxyl protons allowed for both Olsa nanoparticles and Olsa-RVRR to be readily detected (Figure 12e). MRI results have reflected a 15- and 6.5-fold increase in CEST signal in vitro and in vivo, respectively, in comparison to free Olsa. Consequential to the extended periods of drug exposure and improved intracellular retention, Olsa-RVRR demonstrated 20- and 5.2-fold increased cytotoxicity toward HCT116 tumor cells in vitro (Figure 12f) and HCT116

murine xenografts in vivo (Figure 12g), respectively. Intriguingly, the work also claimed an outstanding “theranostic correlation” between the observed therapeutic response and imaging signal ( $R^2 = 0.97$ ). As such, the presented furin-activated MRI-detectable strategy has shown great potential in the further development of theranostic platforms for enhanced image-guided cancer therapy.

On the other hand, Gianneschi and co-workers reported enzyme-transformable nanoparticles for extended retention and targeted accumulation in heart tissues after myocardial infarction (MI)<sup>123</sup> (Figure 13a). The nanoparticles were specially engineered to respond to MMPs present in acute MI, in which they favorably transform from discrete micellar morphologies to network-like scaffolds (Figure 13b). Based with a polynorbornene backbone, the designed fluorescent nanoparticles are composed of brush peptide–polymer amphiphiles (PPAs) conjugated with MMP-2/-9-specific peptide recognition sequences. Intravenous (IV) injection of the enzyme-responsive nanoparticles enabled its free circulation in the bloodstream until they enter an infarct via a post-MI leaky vasculature, in which the nanoparticles will accumulate and spontaneously self-assemble at the injury for approximately 28 days (Figure 13c). The minimally invasive nature of this unique delivery approach could potentially preclude the current use of dangerous intramyocardial injections and provide immediate therapeutic relief post-MI. Subsequently, the same group further adapted their MMP-activated nanoparticle strategy as a delivery platform for sustained chemotherapeutic release observed with low toxicity.<sup>124</sup> Nanoparticles adopting micellar morphologies were once again constructed via direct diblock copolymerization with paclitaxel (PTX) as the hydrophobic core and MMP

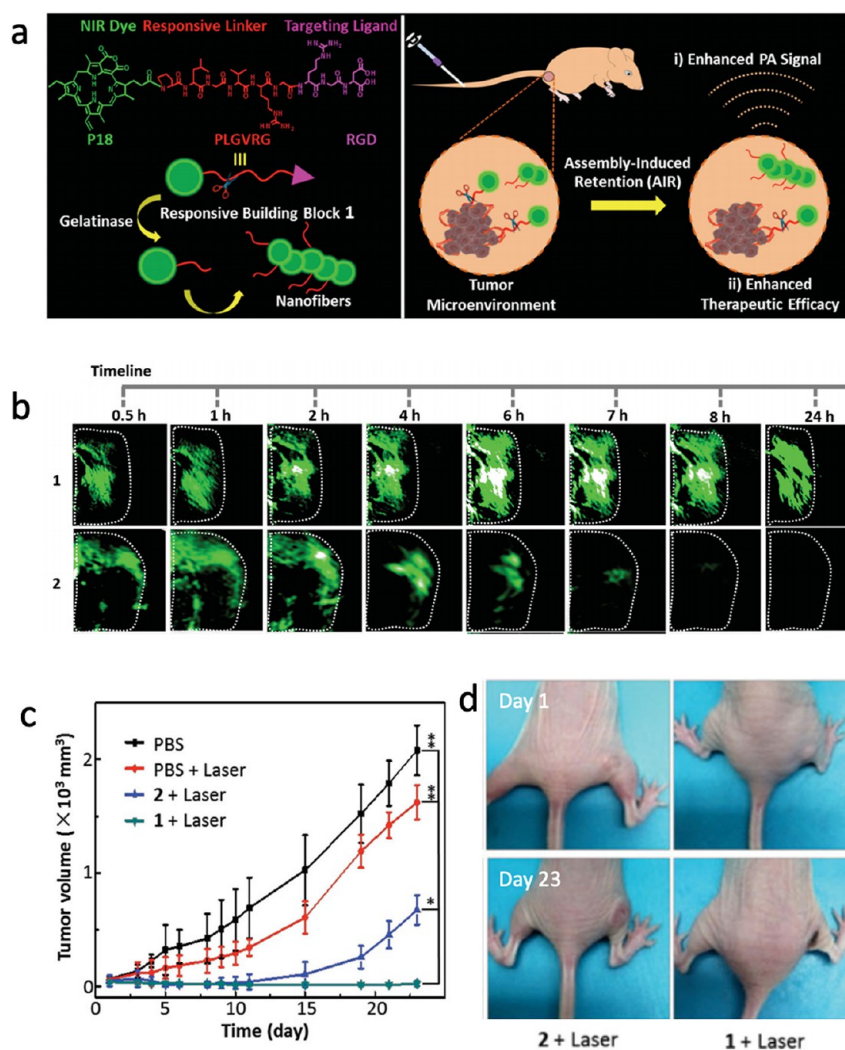


**Figure 15.** (a) Chemical structure of P18-PLGVRGRGD and schematic illustration of gelatinase-responsive construction of nanofibers for improved PA imaging and therapeutic efficacy. (b) Real-time photoacoustic images of tumor site up to 24 h postinjection. (c) Time-dependent tumor volume change of different treatments. (d) Representative images of tumor size before and after different treatment. (1, P18-PLGVRGRGD; 2, non-gelatinase-responsive control). Panels a–d reproduced with permission from ref 126. Copyright 2015 Wiley-VCH.

peptide recognition substrates on the micellar surface. When subjected to microenvironments upregulated with MMP activity, the nanoparticles shed their peptide shell and undergo a dramatic morphological change from 20 nm discrete spherical micelles to micrometer-scale assemblies (Figure 13d). Nanoparticle-bound PTX would gradually be released from the scaffold via hydrolysis, demonstrating an outstanding stunt in tumor growth for approximately 12 days post-intratatumoral administration (Figure 13e). Intriguingly, complete remission was even reported for one of the tested subjects two months post-treatment. In contrast, there were no significant differences between the MMP nonresponsive group and other controls throughout the entire observation period, demonstrating the necessity of a molecular transformation in order for the materials to function. In addition, mice IV-injected with MMP-responsive nanoparticles showed successful suppression of tumor growth even after 2 weeks post-treatment (Figure 13f), whereas despite experiencing rapid proliferation 10 days postinjection, most of the saline cohort were observed with near-lethal tumor volumes just 4 days thereafter. Furthermore, not only did the observed tumor suppression effect of MMP-responsive nanoparticles almost

parallel to that of clinical PTX, the maximum tolerated dose (MTD) observed was also an astounding 16 times higher than clinical PTX before inducing any overt clinical toxicity apart from a weight loss of 10% on day 1 with full recovery observed within the next 3 days (Figure 13g). This implies that, at comparable dosages, the proposed MMP-9-activated strategy has significantly reduced toxicity, which potentially enhances its therapeutic efficacy compared to clinical PTX. This work has provided a new perspective into the design of drug-delivering nanomaterials by virtue of an enzyme-activated morphological transformation to guide the in vivo accumulation of drugs for improved therapeutic efficacy and safety by limiting off-target toxicity.

### 3.3. Self-Assemblies for Photosensitizer Delivery.

Besides the delivery of drugs, photosensitizers can also be encapsulated and efficiently delivered to targeted tumor sites for photothermal and photodynamic therapy. Xing and co-workers have developed a novel microenvironment-sensitive strategy for tumor localization of cathepsin B-responsive upconversion nanocrystals (CRUN)<sup>125</sup> (Figure 14a). Upon specific proteolytic cleavage by cathepsin B overexpressed in tumor microenvironments, the exposed cysteine and 2-

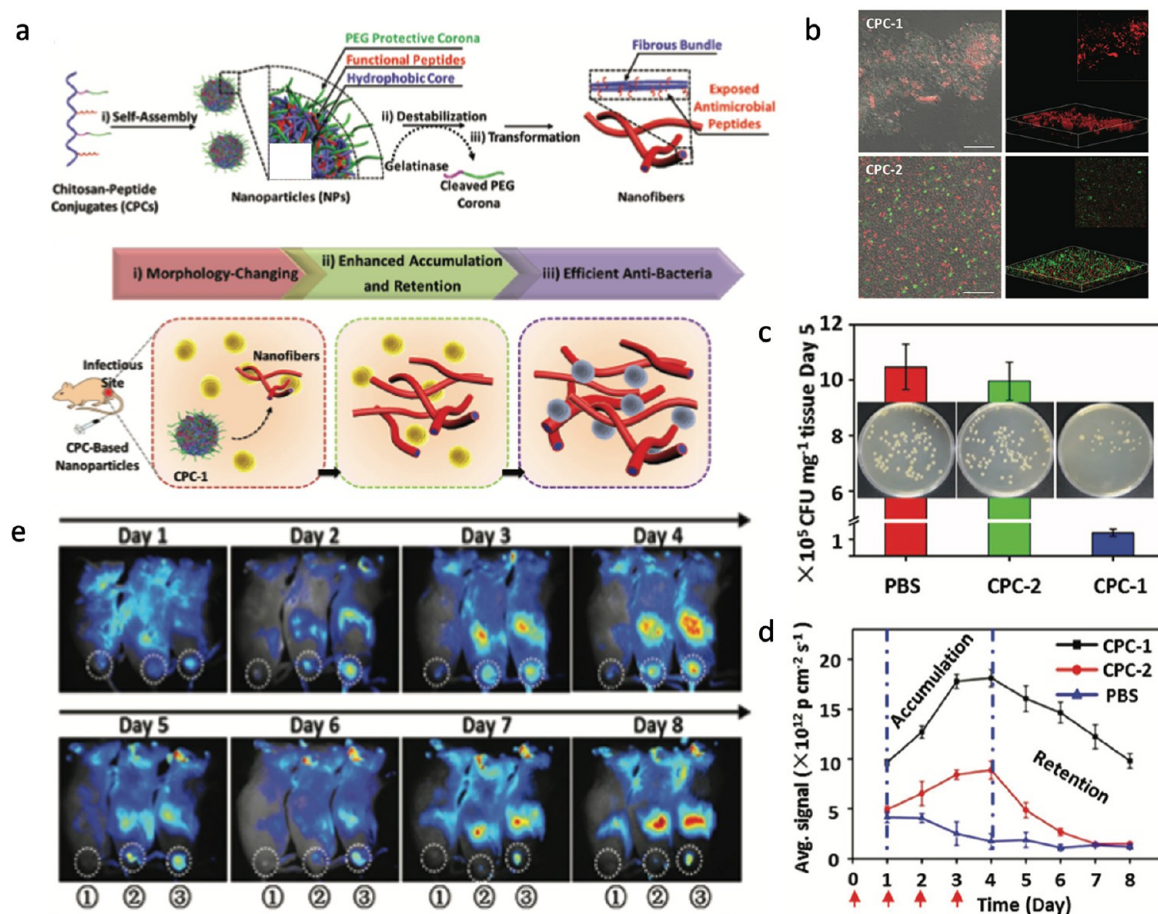


**Figure 16.** (a) Schematic illustration of the self-assembly of CPCs and the principle of enzyme-induced morphology transformation. (b) Confocal microscope images of live/dead cell staining demonstrating the difference in killing efficiency of CPC-1 and CPC-2 upon exposure to gelatinase-positive bacteria. (c) Quantification of surviving *S. aureus* in infected tissues on day 5 and their respective bacteria colonies. (d) Average fluorescence signals at the infected sites at different times. Red arrows indicate injection at days 0, 1, 2, and 3. (e) In vivo optical imaging of *S. aureus*-bearing mice after different treatments. White circles indicate infectious sites. (1, PBS (control); 2, CPC-2; 3, CPC-1). Panels a–e reproduced with permission from ref 127. Copyright 2017 Wiley-VCH.

cyanobenzothiazole of neighboring particles covalently cross-link to induce aggregations of CRUN specifically at tumor sites. This enzyme-activated cross-linking of CRUN led to an effective increase in upconversion emission when irradiated, consequently amplifying the reactive oxygen ( $^1\text{O}_2$ ) production for enhanced photodynamic therapeutic effects (Figure 14b). Encouraged by the favorable results in vitro, the in vivo theranostic efficacy of CRUN was examined via an intratumoral injection into nude mice implanted with cathepsin B overexpressing tumor. The results have shown a significant increase in photoacoustic intensity 4 h postinjection compared to the signal prior to the injection. Additionally, CRUN injected tumors showed a 30% decrease in photoacoustic intensity than those injected with non-cathepsin B-responsive upconversion nanocrystals (NCRUNs), suggesting successful enzyme-activated aggregation in vivo (Figure 14c). Furthermore, CRUN-mediated PDT treatment significantly inhibited tumor growth in group 1, compared to that of group 2 injected with NCRUN and two other control groups, indicating that enzyme-triggered aggregation at the tumor site played an indispensable role in enhancing the therapeutic outcomes (Figure 14d). Subsequently, folic acid affinity ligands were further conjugated to CRUN (FA-PEG@CRUN) to enhance the tumor uptake efficiency for subsequent in vivo studies

administered via intravenous injection. As expected, the tumors injected with FA-PEG@CRUN displayed more effective inhibition than those injected without the surface modification under the same conditions. More notably, the presence of a pork tissue to mimic clinical skin significantly compromised the therapeutic efficacy at 660 nm irradiation compared to that at 808 nm NIR irradiation, demonstrating the profound merits of deep tissue penetration for NIR laser-mediated tumor treatment (Figure 14e). The findings have demonstrated great potential in offering a multimodality solution for site-specific tumor treatment and effective molecular sensing.

Wang and co-workers have designed a small molecule peptide precursor (P18-PLGVRGRGD) sensitive toward gelatinase for improved tumor therapeutic efficacy and enhanced photoacoustic imaging<sup>126</sup> (Figure 15a). The structure of the small molecule peptide precursor comprises functional purpurin 18 (P18) molecule, peptide sequence (PLGVRG) responsive toward gelatinase, and targeting ligand (RGD) to associate with overexpressed  $\alpha v \beta 3$  integrins on tumor cell membranes. Initially, the hydrophilic precursors readily diffused, extravasated, and targeted cancer cells in the physiological environment. Overexpression of gelatinase in the tumor microenvironment cleaves the responsive peptide linker selectively, resulting in residues with enhanced hydrophobicity

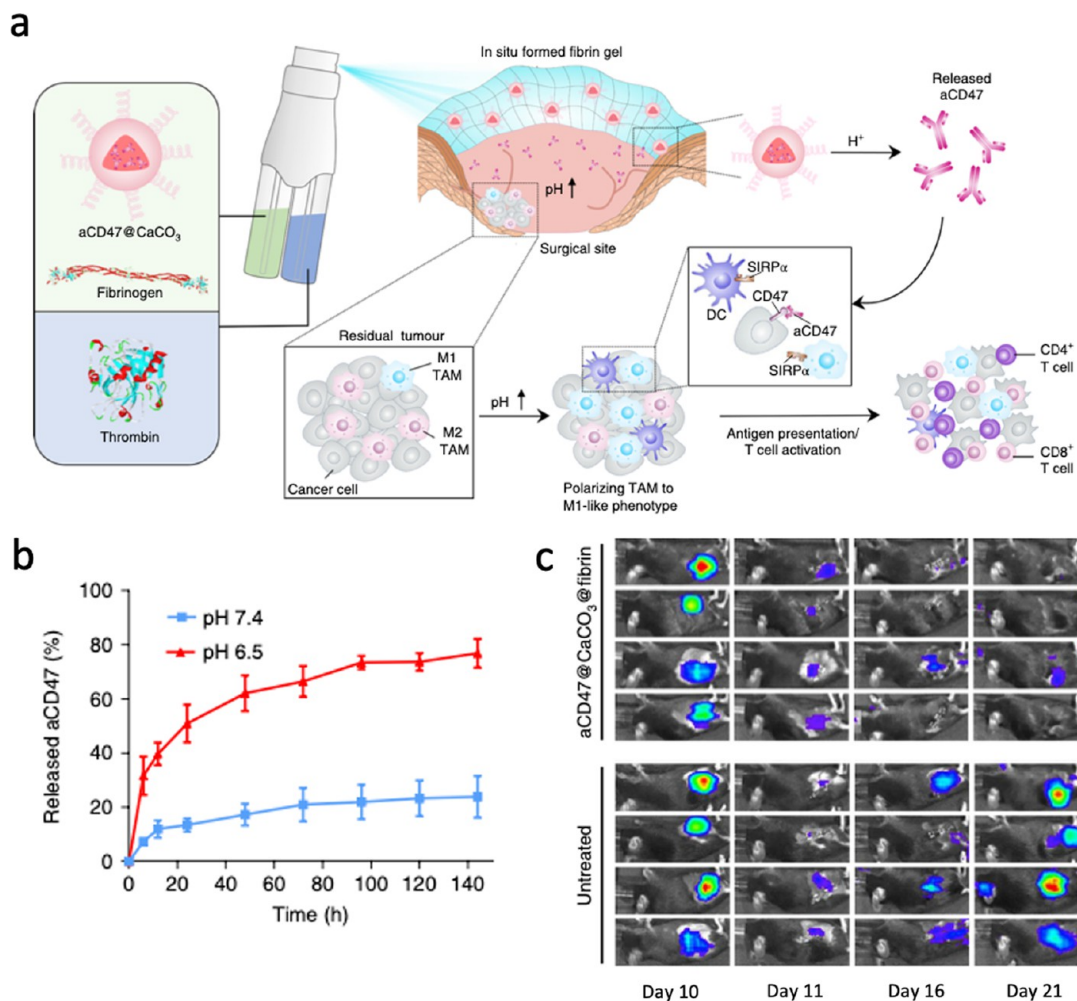


**Figure 17.** (a) Schematic illustration showing the in situ sprayed bioresponsive fibrin gel containing aCD47@CaCO<sub>3</sub> nanoparticles within the postsurgery tumor bed. (b) Cumulative release profiles of aCD47 from fibrin in solutions at different pH values. (c) In vivo bioluminescence imaging of tumors after removal of primary tumor, showing aCD47@CaCO<sub>3</sub>@fibrin reducing recurrence of tumors after surgery. Panels a–c reproduced with permission from ref 130. Copyright 2019 Springer Nature.

that subsequently self-assembled at targeted tumor sites with fibrous nanostructures. Due to the assembly-induced retention (AIR) effect, these nanofibers demonstrated prolonged retention time in tumors as seen from the time-dependent photoacoustic signals of treated tumors (Figure 15b). Initially, comparable photoacoustic signal intensities were observed in both tumor sites for the first 2 h. However, the signal for the non-gelatinase-responsive control diminished at 2 h post-injection due to quick clearance from the tumor site. Further quantification of the average photoacoustic signal for the tumor site treated with P18-PLGVRGRGD showed an astounding 16-fold higher intensity than that of the non-gelatinase-responsive control at 8 h postinjection. Intriguingly, long-time retention of the self-assembled scaffold was observed with a half-retention time of nearly 24 h in the tumor site, 6 times more than that of the non-assembling control. In terms of photothermal therapeutic efficacy, the tumor treated with P18-PLGVRGRGD was suppressed entirely after 23 days, in contrast to treatment with the non-gelatinase-responsive control which progressively grew after 10 days under the same irradiation conditions (Figure 15c). Representative images of tumor-bearing mice for each group (Figure 15d) visually validated the improved tumor inhibition capability of P18-PLGVRGRGD owing to the added AIR effect of nanofiber

formation at tumor areas. After the treatment, the anhydride group of P18 is slowly hydrolyzed to become more hydrophilic molecules which resulted in disassembly and eventual excretion. As such, AIR brought about by an in situ formation of supramolecular structures was successfully demonstrated in living systems with great potential in enhancing cancer diagnostics and therapeutics.

**3.4. Other Therapeutic Applications.** In order to effectively combat bacterial infections, a novel antibacterial strategy was developed by Wang and co-workers. Spherical antibacterial nanoparticles were transformed to fibrous structures upon activation by an infection-induced upregulated proteolytic activity to achieve enhanced antibacterial efficacy with prolonged accumulation within infected sites<sup>127</sup> (Figure 16a). The designed chitosan-peptide conjugates (CPCs) endowed with the ability to change morphology in the presence of bacteria secreted gelatinase demonstrated accumulation, retention, and site-specific targeting which enabled improved cytotoxicity and binding capability toward targeted bacteria. The CPCs comprise three components, a chitosan backbone, an antibacterial peptide CGGGKLA-KLA-KLAK (KLAK), and a gelatinase-cleavable peptide (GPL-GVRGC) with poly(ethylene glycol) terminal (EPEG). The CPCs initially adopt spherical nanoparticle morphologies of

about 34 nm in aqueous solutions. Upon coming into contact with an infectious microenvironment, cleavage of the gelatinase-responsive peptide sheds the protective PEG layer, perturbing the hydrophilic/hydrophobic balance. The resulting destabilized nanoparticles then spontaneously reorganize into fibrous structures via chain–chain interaction of chitosan, exposing the  $\alpha$ -helical structures of KLAK due to its new morphology. Inevitable disruption of bacterial cell membranes would occur due to multivalent cooperative electrostatic interactions with KLAK, resulting in higher observed cytotoxicity than nontransformable CPCs as seen from the obtained live/dead cell staining data (Figure 16b) and quantification of surviving *S. aureus* in infected tissues (Figure 16c). Further in vivo experiments with *S. aureus*-bearing mice have revealed higher accumulation of morphology-changing CPCs (CPC-1) at infected regions compared to their unchanging analogues (CPC-2) (Figure 16d). Moreover, due to unique characteristics of the molecular design made possible with the in situ morphological transition, the half-retention time observed for CPC-1 was an astounding 4 days, while their unresponsive analogues rapidly excreted in less than a day (Figure 16e). As such, this pathological environment-driven construction of polymer–peptide assemblies has offered a novel strategy in designing high-performance nanomaterials with improved binding affinity, effective accumulation, and prolonged retention for an enhanced antibacterial effect, therefore making great contribution toward developments in treating lethal bacterial infections.

Intriguingly, protease-activated self-assemblies have also been further adapted to facilitate the recovery of wounds due to their ability in forming gel-like materials with blood clotting properties for sustained release of therapeutic agents to aid wound recovery. Thrombin is a serine protease playing essential physiological roles in the regulation of hemostasis and maintenance of blood coagulation. Upon activation from prothrombin, thrombin converts fibrinogen to fibrin, which in combination with platelets in blood results in the formation of clots.<sup>128</sup> Inspired by the specific, highly active, and well-defined recognition sequence of this blood clotting enzyme, Soellner and co-workers proposed the detection of proteolytic thrombin activity via an in situ enzymatic gelation with potential practical therapeutic applications.<sup>129</sup> Three hydrophilic D-amino acids and an oligo(ethylene glycol) unit were conjugated to the N-terminus of a thrombin recognition sequence in order to improve the solubility of the peptide gelator and avoid premature gelation prior to the enzymatic cleavage. Upon exposure to thrombin, the peptide gelator is released from its hydrophilic moiety, forming a translucent gel within 10 min. To emphasize the potential practical applications of this gelation strategy, the group successfully demonstrated artificial blood clots in human blood plasma, claiming useful applications in promoting blood coagulation in bandages to treat severe trauma. Intuitively, Gu and co-workers recently developed a spray-on therapeutic gel technique to help with postsurgical cancer immunotherapy. The in situ formation of the therapeutic gel is specially engineered to not only prevent development of distant tumors at tumor resection sites but also inhibit local tumor recurrence after surgery<sup>130</sup> (Figure 17a). As proposed, a solution of pure thrombin enzyme and a solution of fibrinogen mixed with calcium carbonate ( $\text{CaCO}_3$ ) nanoparticles loaded with therapeutic agents were initially contained in two separate chambers of a spray bottle. Upon coadministration at a surgical wound, the enzymatic reaction

between fibrinogen and thrombin results in the in situ formation of a fibrin gel.  $\text{CaCO}_3$  nanoparticles embedded in the gel matrix would aid the controlled release of therapeutics (Figure 17b) and regulate the acidic environment of the inflamed tumor resection site by scavenging  $\text{H}^+$ , thereby promoting an antitumor immune response to better facilitate the recovery process (Figure 17c). Although not activated by the aberrant overexpression of protease in diseased tissues, this novel strategy in developing protease-activated construction of therapeutic fibrin gel holds promising potential for practical applications in sustained and controlled release of therapeutic agents at open wounds and surgical sites to facilitate the recovery process.

#### 4. CONCLUSION AND PERSPECTIVES

In view of all of the recent developments in protease-activated self-assemblies for imaging and therapeutic applications, we easily find a new trend in the increasing popularity of developing in situ self-assembled nanostructures, where the administered nanomaterials change their structures, morphologies, and functionalities at a biointerface, forming more stable scaffolds to adapt to the special application environment. Although conventional strategies employing nanostructures assembled ex situ have demonstrated increased bioavailability and targetability due to enhanced permeability and retention (EPR) and multivalent effects, their preassembled structures sometimes suffer from intrinsic instability under complicated physiological conditions in vivo. Exploiting the dynamic nature of molecular self-assembly, in situ morphology transformation has shown promising results in the prolonged retention of imaging and therapeutic agents, finding potential applications in long-term imaging and sustained therapeutic release. Furthermore, the manifestation of most diseases originate from molecular malfunctions too insignificant to be detectable by existing diagnostic techniques. Molecular-level events such as the overexpression of a disease-related protease can be amplified by inducing an aggregation to better facilitate early detection. The developments presented in this review have successfully demonstrated in situ assembly of nanostructures activated by specific biological stimuli as a promising strategy with untapped potential for further development of imaging and therapeutic materials with enhanced stability and sensitivity.

In terms of the enzymatic nature, proteases have experienced increased research interest as therapeutic targets in recent years due to their highly specific catalytic activity in only cleaving substrates that contain unique amino acid sequences corresponding to the architecture of their active site. Enzymes such as phosphatase or esterase, whose enzymatic activities have previously been heavily exploited with the well-known EISA strategy, often require the additional conjugation of a more specific targeting moiety to improve their binding affinity and selectivity in vivo. In contrast, the innate substrate specificity of a proteolytic active site makes protease a more promising contender for future developments of in situ enzyme-activated self-assemblies in vivo.

To date, tremendous efforts have been devoted in the development of imaging applications for protease-activated self-assemblies to detect tumor and abnormal enzymatic activity due to their unique characteristics. Typically, the upregulated proteolytic activity is first used to “turn on” the signal, while the induced aggregation amplifies it subsequently. However, despite the promising abilities of these nanoprobes

developed over the decade, their practical applications and clinical translation are still faced with several challenges such as poor stability, inferior sensitivity, and specificity in vivo compared to commercially available probes. Several strategies have been devised to mitigate these issues. Unnatural amino acids can be incorporated outside the proteolytic recognition site to improve the metabolic stability of the probes in vivo. The sensitivity of the response signal can be enhanced by combining multiple imaging modalities into the same probe, while the specificity can be improved by further modification with a targeting moiety to selectively optimize the binding affinity toward diseased tissues in vivo. There should also be a standardized procedure to evaluate the toxicity of imaging probes in vivo so as to improve the efficiency for clinical translations. These issues need to be urgently addressed in future studies in order to unleash the full potential of these imaging probes.

Compared to imaging applications, the therapeutic uses of protease-activated self-assemblies are not as well-developed. However, this review has summarized quite a few interesting works published in recent years. For example, protease-activated assembled structures can act as drug carriers with low innate cytotoxicity without the influence of the encapsulated therapeutic drug. The nontoxic nature of the nanocarriers was seen to improve the therapeutic effect of the anticancer drug. Additionally, prodrugs conjugated to enzyme-activated assembly scaffolds also showed much lower toxicity at equivalent doses for equivalent therapeutic efficacy compared to a clinically available drug. However, the complexity of the physiological environment should not be overlooked as it can lead to low stability of the therapeutic agent or premature drug leakage from the carrier, causing complications in further practical applications. In order to optimize the therapeutic efficacy, unnatural amino acids can similarly be incorporated outside the proteolytic recognition site to improve the metabolic stability of the therapeutic agents and drug carriers in vivo. Furthermore, there is also a lack of effective observation techniques and strategies with the ability to monitor and evaluate real-time morphological changes and characterize the dynamic nature of peptide assemblies in living cells and organisms. This is a formidable challenge that needs to be addressed urgently as well in order to prove that the developed therapeutic agents can have more practical applications in the living system. Last but not least, more detailed pharmacokinetic and pharmacodynamic studies should be conducted on the assembled scaffolds, particularly in the extensive evaluation of post-therapeutic degradability and excretion so as to facilitate potential clinical translations.

In general, most of the developments to date mainly targeted tumor-associated proteases, thus finding useful applications toward tumor imaging and therapeutics. However, the rising interests in protease expressions relating to other biomedical aspects such as bacterial infections, neurodegenerative disorders, and wound recovery have emerged very recently. We have only just scratched the surface and wholeheartedly believe that the continuous collaborative efforts among multidisciplinary researchers will unveil more detailed biological investigations on the many roles played by proteases in the physiological environment, hence bringing about more useful practical applications that will benefit us all in the near future.

## AUTHOR INFORMATION

### Corresponding Author

**Bengang Xing** – Division of Chemistry and Biological Chemistry, School of Physical & Mathematical Sciences and School of Chemical & Biomedical Engineering, Nanyang Technological University, 637371, Singapore; [orcid.org/0000-0002-8391-1234](https://orcid.org/0000-0002-8391-1234); Email: [bengang@ntu.edu.sg](mailto:bengang@ntu.edu.sg)

### Authors

**Germain Kwek** – Division of Chemistry and Biological Chemistry, School of Physical & Mathematical Sciences, Nanyang Technological University, 637371, Singapore

**Thang Cong Do** – Division of Chemistry and Biological Chemistry, School of Physical & Mathematical Sciences, Nanyang Technological University, 637371, Singapore

**Xiaoling Lu** – International Nanobody Research Centre of Guangxi, Guangxi Medical University, Nanning, Guangxi 530021, China

**Jun Lin** – State Key Laboratory of Rare Earth Resource Utilization, Changchun Institute of Applied Chemistry, Chinese Academy of Sciences, Changchun 130022, China

Complete contact information is available at:  
<https://pubs.acs.org/10.1021/acsabm.0c01340>

### Notes

The authors declare no competing financial interest.

## ACKNOWLEDGMENTS

B.X. acknowledges the financial support from Tier 1 RG5/18 (S), RG6/20, MOE 2017-T2-2-110, Start-Up Grant (SUG), A\*Star SERC A1983c0028 (M4070319), A20E5c0090, and the National Natural Science Foundation of China (NSFC; No. 51929201)

## REFERENCES

- (1) Bovey, F. *Macromolecules: An introduction to polymer science*; Elsevier, 2012.
- (2) Bretscher, M. S. The Molecules of the Cell Membrane. *Sci. Am.* **1985**, 253 (4), 100–109.
- (3) Watson, J. D.; Crick, F. H. C. Molecular Structure of Nucleic Acids: A Structure for Deoxyribose Nucleic Acid. *Nature* **1953**, 171 (4356), 737–738.
- (4) Fetrow, J. S.; Palumbo, M. J.; Berg, G. Patterns, structures, and amino acid frequencies in structural building blocks, a protein secondary structure classification scheme. *Proteins: Struct., Funct., Genet.* **1997**, 27 (2), 249–271.
- (5) Ren, C.; Wang, Z.; Wang, Q.; Yang, C.; Liu, J. Self-Assembled Peptide-Based Nanoprobes for Disease Theranostics and Disease-Related Molecular Imaging. *Small Methods* **2020**, 4 (4), 1900403.
- (6) Hu, Y.; Wang, Y.; Wen, X.; Pan, Y.; Cheng, X.; An, R.; Gao, G.; Chen, H.-Y.; Ye, D. Responsive Trimodal Probes for In Vivo Imaging of Liver Inflammation by Coassembly and GSH-Driven Disassembly. *Research* **2020**, 2020, 4087069.
- (7) Qi, G.-B.; Gao, Y.-J.; Wang, L.; Wang, H. Self-Assembled Peptide-Based Nanomaterials for Biomedical Imaging and Therapy. *Adv. Mater.* **2018**, 30 (22), 1703444.
- (8) An, R.; Cheng, X.; Wei, S.; Hu, Y.; Sun, Y.; Huang, Z.; Chen, H.-Y.; Ye, D. Smart Magnetic and Fluorogenic Photosensitizer Nanoassemblies Enable Redox-Driven Disassembly for Photodynamic Therapy. *Angew. Chem., Int. Ed.* **2020**, 59 (46), 20636–20644.
- (9) Walsh, C. Enabling the chemistry of life. *Nature* **2001**, 409 (6817), 226–31.
- (10) Qi, S. Y.; Groves, J. T.; Chakraborty, A. K. Synaptic pattern formation during cellular recognition. *Proc. Natl. Acad. Sci. U. S. A.* **2001**, 98 (12), 6548–6553.

- (11) Scherzinger, E.; Sittler, A.; Schweiger, K.; Heiser, V.; Lurz, R.; Hasenbank, R.; Bates, G. P.; Lehrach, H.; Wanker, E. E. Self-assembly of polyglutamine-containing huntingtin fragments into amyloid-like fibrils: implications for Huntington's disease pathology. *Proc. Natl. Acad. Sci. U. S. A.* **1999**, *96* (8), 4604–9.
- (12) Schnur, J. M. Lipid Tubules: A Paradigm for Molecularly Engineered Structures. *Science* **1993**, *262* (5140), 1669–1676.
- (13) Timpl, R.; Brown, J. C. Supramolecular assembly of basement membranes. *BioEssays* **1996**, *18* (2), 123–132.
- (14) Whitesides, G.; Mathias, J.; Seto, C. Molecular self-assembly and nanochemistry: a chemical strategy for the synthesis of nanostructures. *Science* **1991**, *254* (5036), 1312–1319.
- (15) Spruell, J. M.; Hawker, C. J. Triggered structural and property changes in polymeric nanomaterials. *Chemical Science* **2011**, *2* (1), 18–26.
- (16) Yang, Z.; Liang, G.; Guo, Z.; Guo, Z.; Xu, B. Intracellular Hydrogelation of Small Molecules Inhibits Bacterial Growth. *Angew. Chem., Int. Ed.* **2007**, *46* (43), 8216–8219.
- (17) Chen, Y.; Liang, G. Enzymatic self-assembly of nanostructures for theranostics. *Theranostics* **2012**, *2* (2), 139–147.
- (18) Kunjachan, S.; Ehling, J.; Storm, G.; Kiessling, F.; Lammers, T. Noninvasive Imaging of Nanomedicines and Nanotheranostics: Principles, Progress, and Prospects. *Chem. Rev.* **2015**, *115* (19), 10907–10937.
- (19) French, K. M.; Somasuntharam, I.; Davis, M. E. Self-assembling peptide-based delivery of therapeutics for myocardial infarction. *Adv. Drug Delivery Rev.* **2016**, *96*, 40–53.
- (20) Han, K.; Liu, Y.; Yin, W.-N.; Wang, S.-B.; Xu, Q.; Zhuo, R.-X.; Zhang, X.-Z. A FRET-Based Dual-Targeting Theranostic Chimeric Peptide for Tumor Therapy and Real-time Apoptosis Imaging. *Adv. Healthcare Mater.* **2014**, *3* (11), 1765–1768.
- (21) Huang, F.; Wang, J.; Qu, A.; Shen, L.; Liu, J.; Liu, J.; Zhang, Z.; An, Y.; Shi, L. Maintenance of amyloid  $\beta$  peptide homeostasis by artificial chaperones based on mixed-shell polymeric micelles. *Angew. Chem., Int. Ed.* **2014**, *53* (34), 9885–90.
- (22) Liang, G.; Ren, H.; Rao, J. A biocompatible condensation reaction for controlled assembly of nanostructures in living cells. *Nat. Chem.* **2010**, *2* (1), 54–60.
- (23) Ye, D.; Liang, G.; Ma, M. L.; Rao, J. Controlling Intracellular Macrocyclization for the Imaging of Protease Activity. *Angew. Chem., Int. Ed.* **2011**, *50* (10), 2275–2279.
- (24) Collier, J. H.; Rudra, J. S.; Gasiorowski, J. Z.; Jung, J. P. Multi-component extracellular matrices based on peptide self-assembly. *Chem. Soc. Rev.* **2010**, *39* (9), 3413–3424.
- (25) Lam, K. S.; Salmon, S. E.; Hersh, E. M.; Hruby, V. J.; Kazmierski, W. M.; Knapp, R. J. A new type of synthetic peptide library for identifying ligand-binding activity. *Nature* **1991**, *354* (6348), 82–84.
- (26) Ren, C.; Zhang, J.; Chen, M.; Yang, Z. Self-assembling small molecules for the detection of important analytes. *Chem. Soc. Rev.* **2014**, *43* (21), 7257–7266.
- (27) Wang, J.; Liu, K.; Xing, R.; Yan, X. Peptide self-assembly: thermodynamics and kinetics. *Chem. Soc. Rev.* **2016**, *45* (20), 5589–5604.
- (28) Zelzer, M.; Ulijn, R. V. Next-generation peptide nanomaterials: molecular networks, interfaces and supramolecular functionality. *Chem. Soc. Rev.* **2010**, *39* (9), 3351–7.
- (29) Fjell, C. D.; Hiss, J. A.; Hancock, R. E.; Schneider, G. Designing antimicrobial peptides: form follows function. *Nat. Rev. Drug Discovery* **2012**, *11* (1), 37–51.
- (30) Merrifield, R. B. Solid Phase Peptide Synthesis. I. The Synthesis of a Tetrapeptide. *J. Am. Chem. Soc.* **1963**, *85* (14), 2149–2154.
- (31) Chen, S.; Lei, Q.; Li, S.-Y.; Qin, S.-Y.; Jia, H.-Z.; Cheng, Y.-J.; Zhang, X.-Z. Fabrication of dual responsive co-delivery system based on three-armed peptides for tumor therapy. *Biomaterials* **2016**, *92*, 25–35.
- (32) Han, K.; Zhang, W.-Y.; Zhang, J.; Lei, Q.; Wang, S.-B.; Liu, J.-W.; Zhang, X.-Z.; Han, H.-Y. Acidity-Triggered Tumor-Targeted Chimeric Peptide for Enhanced Intra-Nuclear Photodynamic Therapy. *Adv. Funct. Mater.* **2016**, *26* (24), 4351–4361.
- (33) Cozzzone, A. J. Proteins: Fundamental Chemical Properties. *eLS* **2010**, DOI: 10.1002/9780470015902.a0001330.pub2
- (34) Zhang, L.; Wang, T.; Shen, Z.; Liu, M. Chiral Nano-architectonics: Towards the Design, Self-Assembly, and Function of Nanoscale Chiral Twists and Helices. *Adv. Mater.* **2016**, *28* (6), 1044–1059.
- (35) Aggeli, A.; Nyrkova, I. A.; Bell, M.; Harding, R.; Carrick, L.; McLeish, T. C. B.; Semenov, A. N.; Boden, N. Hierarchical self-assembly of chiral rod-like molecules as a model for peptide  $\beta$ -sheet tapes, ribbons, fibrils, and fibers. *Proc. Natl. Acad. Sci. U. S. A.* **2001**, *98* (21), 11857–11862.
- (36) Zhao, X.; Zhang, S. Designer Self-Assembling Peptide Materials. *Macromol. Biosci.* **2007**, *7* (1), 13–22.
- (37) Kunitake, T. Synthetic Bilayer Membranes: Molecular Design, Self-Organization, and Application. *Angew. Chem., Int. Ed. Engl.* **1992**, *31* (6), 709–726.
- (38) Ulijn, R. V.; Smith, A. M. Designing peptide based nanomaterials. *Chem. Soc. Rev.* **2008**, *37* (4), 664–675.
- (39) Yang, Z.; Liang, G.; Xu, B. Enzymatic Hydrogelation of Small Molecules. *Acc. Chem. Res.* **2008**, *41* (2), 315–326.
- (40) Sun, X.; Li, Y.; Liu, T.; Li, Z.; Zhang, X.; Chen, X. Peptide-based imaging agents for cancer detection. *Adv. Drug Delivery Rev.* **2017**, *110–111*, 38–51.
- (41) Zhan, J.; Cai, Y.; He, S.; Wang, L.; Yang, Z. Tandem Molecular Self-Assembly in Liver Cancer Cells. *Angew. Chem., Int. Ed.* **2018**, *57* (7), 1813–1816.
- (42) Feng, Z.; Wang, H.; Zhou, R.; Li, J.; Xu, B. Enzyme-Instructed Assembly and Disassembly Processes for Targeting Downregulation in Cancer Cells. *J. Am. Chem. Soc.* **2017**, *139* (11), 3950–3953.
- (43) Kuang, Y.; Shi, J.; Li, J.; Yuan, D.; Alberti, K. A.; Xu, Q.; Xu, B. Pericellular hydrogel/nanonets inhibit cancer cells. *Angew. Chem., Int. Ed.* **2014**, *53* (31), 8104–8107.
- (44) Li, J.; Gao, Y.; Kuang, Y.; Shi, J.; Du, X.; Zhou, J.; Wang, H.; Yang, Z.; Xu, B. Dephosphorylation of D-peptide derivatives to form biofunctional, supramolecular nanofibers/hydrogels and their potential applications for intracellular imaging and intratumoral chemotherapy. *J. Am. Chem. Soc.* **2013**, *135* (26), 9907–9914.
- (45) Wang, H.; Feng, Z.; Wang, Y.; Zhou, R.; Yang, Z.; Xu, B. Integrating Enzymatic Self-Assembly and Mitochondria Targeting for Selectively Killing Cancer Cells without Acquired Drug Resistance. *J. Am. Chem. Soc.* **2016**, *138* (49), 16046–16055.
- (46) Zhou, J.; Du, X.; Li, J.; Yamagata, N.; Xu, B. Taurine Boosts Cellular Uptake of Small d-Peptides for Enzyme-Instructed Intracellular Molecular Self-Assembly. *J. Am. Chem. Soc.* **2015**, *137* (32), 10040–10043.
- (47) Zhou, J.; Du, X.; Wang, J.; Yamagata, N.; Xu, B. Enzyme-Instructed Self-Assembly of Peptides Containing Phosphoserine to Form Supramolecular Hydrogels as Potential Soft Biomaterials. *Front. Chem. Sci. Eng.* **2017**, *11* (4), 509–515.
- (48) Rawlings, N. D.; Barrett, A. J.; Thomas, P. D.; Huang, X.; Bateman, A.; Finn, R. D. The MEROPS database of proteolytic enzymes, their substrates and inhibitors in 2017 and a comparison with peptidases in the PANTHER database. *Nucleic Acids Res.* **2018**, *46* (D1), D624–d632.
- (49) Drag, M.; Salvesen, G. S. Emerging principles in protease-based drug discovery. *Nat. Rev. Drug Discovery* **2010**, *9* (9), 690–701.
- (50) Poreba, M. Protease-activated prodrugs: strategies, challenges, and future directions. *FEBS J.* **2020**, *287* (10), 1936–1969.
- (51) Akkari, L.; Gocheva, V.; Quick, M. L.; Kester, J. C.; Spencer, A. K.; Garfall, A. L.; Bowman, R. L.; Joyce, J. A. Combined deletion of cathepsin protease family members reveals compensatory mechanisms in cancer. *Genes Dev.* **2016**, *30* (2), 220–32.
- (52) Egbring, R.; Schmidt, W.; Fuchs, G.; Havemann, K. Demonstration of granulocytic proteases in plasma of patients with acute leukemia and septicemia with coagulation defects. *Blood* **1977**, *49* (2), 219–231.

- (53) Lah, T. T.; Kalman, E.; Najjar, D.; Gorodetsky, E.; Brennan, P.; Somers, R.; Daskal, I. Cells producing cathepsins D, B, and L in human breast carcinoma and their association with prognosis. *Hum. Pathol.* **2000**, *31* (2), 149–60.
- (54) Zou, P.; Chen, W.-T.; Sun, T.; Gao, Y.; Li, L.-L.; Wang, H. Recent advances: peptides and self-assembled peptide-nanosystems for antimicrobial therapy and diagnosis. *Biomater. Sci.* **2020**, *8* (18), 4975–4996.
- (55) Nixon, R. A. The role of autophagy in neurodegenerative disease. *Nat. Med.* **2013**, *19* (8), 983–97.
- (56) Carl, P. L.; Chakravarty, P. K.; Katzenellenbogen, J. A.; Weber, M. J. Protease-activated “prodrugs” for cancer chemotherapy. *Proc. Natl. Acad. Sci. U. S. A.* **1980**, *77* (4), 2224–2228.
- (57) Choi, K. Y.; Swierczewska, M.; Lee, S.; Chen, X. Protease-Activated Drug Development. *Theranostics* **2012**, *2* (2), 156–178.
- (58) Lehar, S. M.; Pillow, T.; Xu, M.; Staben, L.; Kajihara, K. K.; Vandlen, R.; DePalatis, L.; Raab, H.; Hazenbos, W. L.; Hiroshi Morisaki, J.; Kim, J.; Park, S.; Darwish, M.; Lee, B.-C.; Hernandez, H.; Loyet, K. M.; Lupardus, P.; Fong, R.; Yan, D.; Chalouni, C.; Luis, E.; Khalif, Y.; Plise, E.; Cheong, J.; Lyssikatos, J. P.; Strandh, M.; Koefoed, K.; Andersen, P. S.; Flygare, J. A.; Wah Tan, M.; Brown, E. J.; Mariathasan, S. Novel antibody–antibiotic conjugate eliminates intracellular *S. aureus*. *Nature* **2015**, *527* (7578), 323–328.
- (59) Connors, J. M.; Jurczak, W.; Straus, D. J.; Ansell, S. M.; Kim, W. S.; Gallamini, A.; Younes, A.; Alekseev, S.; Illés, Á.; Picardi, M.; Lech-Maranda, E.; Oki, Y.; Feldman, T.; Smolewski, P.; Savage, K. J.; Bartlett, N. L.; Walewski, J.; Chen, R.; Ramchandren, R.; Zinzani, P. L.; Cunningham, D.; Rosta, A.; Josephson, N. C.; Song, E.; Sachs, J.; Liu, R.; Jolin, H. A.; Huebner, D.; Radford, J. Brentuximab Vedotin with Chemotherapy for Stage III or IV Hodgkin’s Lymphoma. *N. Engl. J. Med.* **2018**, *378* (4), 331–344.
- (60) Tilly, H.; Morschhauser, F.; Bartlett, N. L.; Mehta, A.; Salles, G.; Haioun, C.; Munoz, J.; Chen, A. I.; Kolibaba, K.; Lu, D.; Yan, M.; Penuel, E.; Hirata, J.; Lee, C.; Sharman, J. P. Polatuzumab vedotin in combination with immunochemotherapy in patients with previously untreated diffuse large B-cell lymphoma: an open-label, non-randomised, phase 1b-2 study. *Lancet Oncol.* **2019**, *20* (7), 998–1010.
- (61) Cohen, G. M. Caspases: the executioners of apoptosis. *Biochem. J.* **1997**, *326* (1), 1–16.
- (62) Shi, H.; Kwok, R. T. K.; Liu, J.; Xing, B.; Tang, B. Z.; Liu, B. Real-Time Monitoring of Cell Apoptosis and Drug Screening Using Fluorescent Light-Up Probe with Aggregation-Induced Emission Characteristics. *J. Am. Chem. Soc.* **2012**, *134* (43), 17972–17981.
- (63) Talanian, R. V.; Quinlan, C.; Trautz, S.; Hackett, M. C.; Mankovich, J. A.; Banach, D.; Ghayur, T.; Brady, K. D.; Wong, W. W. Substrate specificities of caspase family proteases. *J. Biol. Chem.* **1997**, *272* (15), 9677–82.
- (64) Yuan, Y.; Kwok, R. T. K.; Tang, B. Z.; Liu, B. Targeted Theranostic Platinum(IV) Prodrug with a Built-In Aggregation-Induced Emission Light-Up Apoptosis Sensor for Noninvasive Early Evaluation of Its Therapeutic Responses in Situ. *J. Am. Chem. Soc.* **2014**, *136* (6), 2546–2554.
- (65) Aggarwal, N.; Sloane, B. F. Cathepsin B: multiple roles in cancer. *Proteomics: Clin. Appl.* **2014**, *8* (5–6), 427–437.
- (66) Duncan, R.; Cable, H. C.; Lloyd, J. B.; Rejmanová, P.; Kopeček, J. Polymers containing enzymatically degradable bonds. 7. Design of oligopeptide side-chains in poly[N-(2-hydroxypropyl)-methacrylamide] copolymers to promote efficient degradation by lysosomal enzymes. *Makromol. Chem.* **1983**, *184* (10), 1997–2008.
- (67) Rejmanová, P.; Kopeček, J.; Pohl, J.; Baudyš, M.; Kostka, V. Polymers containing enzymatically degradable bonds. 8. Degradation of oligopeptide sequences in N-(2-hydroxypropyl)methacrylamide copolymers by bovine spleen cathepsin B. *Makromol. Chem.* **1983**, *184* (10), 2009–2020.
- (68) Han, H.; Jin, Q.; Wang, Y.; Chen, Y.; Ji, J. The rational design of a gemcitabine prodrug with AIE-based intracellular light-up characteristics for selective suppression of pancreatic cancer cells. *Chem. Commun.* **2015**, *51* (98), 17435–17438.
- (69) Yuan, Y.; Zhang, C.-J.; Gao, M.; Zhang, R.; Tang, B. Z.; Liu, B. Specific Light-Up Bioprobe with Aggregation-Induced Emission and Activatable Photoactivity for the Targeted and Image-Guided Photodynamic Ablation of Cancer Cells. *Angew. Chem., Int. Ed.* **2015**, *54* (6), 1780–1786.
- (70) Chien, M. P.; Thompson, M. P.; Barback, C. V.; Ku, T. H.; Hall, D. J.; Gianneschi, N. C. Enzyme-directed assembly of a nanoparticle probe in tumor tissue. *Adv. Mater.* **2013**, *25* (26), 3599–604.
- (71) Edwards, D. R.; Murphy, G. Cancer. Proteases–invasion and more. *Nature* **1998**, *394* (6693), 527–8.
- (72) Chien, M. P.; Carlini, A. S.; Hu, D.; Barback, C. V.; Rush, A. M.; Hall, D. J.; Orr, G.; Gianneschi, N. C. Enzyme-directed assembly of nanoparticles in tumors monitored by in vivo whole animal imaging and ex vivo super-resolution fluorescence imaging. *J. Am. Chem. Soc.* **2013**, *135* (50), 18710–3.
- (73) Shapiro, J.; Sciaky, N.; Lee, J.; Bosshart, H.; Angeletti, R. H.; Bonifacino, J. S. Localization of endogenous furin in cultured cell lines. *J. Histochem. Cytochem.* **1997**, *45* (1), 3–12.
- (74) Thomas, G. Furin at the cutting edge: from protein traffic to embryogenesis and disease. *Nat. Rev. Mol. Cell Biol.* **2002**, *3* (10), 753–766.
- (75) Mbikay, M.; Sirois, F.; Yao, J.; Seidah, N. G.; Chrétien, M. Comparative analysis of expression of the proprotein convertases furin, PACE4, PC1 and PC2 in human lung tumours. *Br. J. Cancer* **1997**, *75* (10), 1509–14.
- (76) Hosaka, M.; Nagahama, M.; Kim, W. S.; Watanabe, T.; Hatsuzawa, K.; Ikemizu, J.; Murakami, K.; Nakayama, K. Arg-X-Lys/Arg-Arg motif as a signal for precursor cleavage catalyzed by furin within the constitutive secretory pathway. *J. Biol. Chem.* **1991**, *266* (19), 12127–12130.
- (77) Bassi, D. E.; Fu, J.; Lopez de Cicco, R.; Klein-Szanto, A. J. Proprotein convertases: “master switches” in the regulation of tumor growth and progression. *Mol. Carcinog.* **2005**, *44* (3), 151–61.
- (78) Cheng, M.; Watson, P. H.; Paterson, J. A.; Seidah, N.; Chrétien, M.; Shiu, R. P. Pro-protein convertase gene expression in human breast cancer. *Int. J. Cancer* **1997**, *71* (6), 966–71.
- (79) Dragulescu-Andrasi, A.; Liang, G.; Rao, J. In vivo bioluminescence imaging of furin activity in breast cancer cells using bioluminescent substrates. *Bioconjugate Chem.* **2009**, *20* (8), 1660–1666.
- (80) Tandon, A. K.; Clark, G. M.; Chamness, G. C.; Chirgwin, J. M.; McGuire, W. L. Cathepsin D and prognosis in breast cancer. *N. Engl. J. Med.* **1990**, *322* (5), 297–302.
- (81) Yan, S.; Sameni, M.; Sloane, B. F. Cathepsin B and human tumor progression. *Biol. Chem.* **1998**, *379* (2), 113–123.
- (82) Cao, C.-y.; Chen, Y.; Wu, F.-z.; Deng, Y.; Liang, G.-l. Caspase-3 controlled assembly of nanoparticles for fluorescence turn on. *Chem. Commun.* **2011**, *47* (37), 10320–10322.
- (83) Cao, C.-Y.; Shen, Y.-Y.; Wang, J.-D.; Li, L.; Liang, G.-L. Controlled intracellular self-assembly of gadolinium nanoparticles as smart molecular MR contrast agents. *Sci. Rep.* **2013**, *3* (1), 1024.
- (84) Liu, X.; Liang, G. Dual aggregation-induced emission for enhanced fluorescence sensing of furin activity in vitro and in living cells. *Chem. Commun.* **2017**, *53* (6), 1037–1040.
- (85) Wang, H.; Chen, P.; Wu, H.; Zou, P.; Wu, J.; Liu, Y.; Liang, G. Furin-Guided Intracellular <sup>68</sup>Ga Nanoparticle Formation Enhancing Tumor MicroPET Imaging. *Anal. Chem.* **2019**, *91* (23), 14842–14845.
- (86) Liu, Y.; Miao, Q.; Zou, P.; Liu, L.; Wang, X.; An, L.; Zhang, X.; Qian, X.; Luo, S.; Liang, G. Enzyme-Controlled Intracellular Self-Assembly of (18)F Nanoparticles for Enhanced MicroPET Imaging of Tumor. *Theranostics* **2015**, *5* (10), 1058–1067.
- (87) Dragulescu-Andrasi, A.; Kothapalli, S.-R.; Tikhomirov, G. A.; Rao, J.; Gambhir, S. S. Activatable Oligomerizable Imaging Agents for Photoacoustic Imaging of Furin-Like Activity in Living Subjects. *J. Am. Chem. Soc.* **2013**, *135* (30), 11015–11022.
- (88) Hai, Z.; Ni, Y.; Saimi, D.; Yang, H.; Tong, H.; Zhong, K.; Liang, G.  $\gamma$ -Glutamyltranspeptidase-Triggered Intracellular Gadolinium

Nanoparticle Formation Enhances the T2-Weighted MR Contrast of Tumor. *Nano Lett.* **2019**, *19* (4), 2428–2433.

(89) Yuan, Y.; Ge, S.; Sun, H.; Dong, X.; Zhao, H.; An, L.; Zhang, J.; Wang, J.; Hu, B.; Liang, G. Intracellular Self-Assembly and Disassembly of 19F Nanoparticles Confer Respective “Off” and “On” 19F NMR/MRI Signals for Legumain Activity Detection in Zebrafish. *ACS Nano* **2015**, *9* (5), 5117–5124.

(90) Ye, D.; Shuhendler, A. J.; Cui, L.; Tong, L.; Tee, S. S.; Tikhomirov, G.; Felsher, D. W.; Rao, J. Bioorthogonal cyclization-mediated in situ self-assembly of small-molecule probes for imaging caspase activity in vivo. *Nat. Chem.* **2014**, *6* (6), 519–526.

(91) Ye, D.; Shuhendler, A. J.; Pandit, P.; Brewer, K. D.; Tee, S. S.; Cui, L.; Tikhomirov, G.; Rutt, B.; Rao, J. Caspase-responsive smart gadolinium-based contrast agent for magnetic resonance imaging of drug-induced apoptosis. *Chemical Science* **2014**, *5* (10), 3845–3852.

(92) Nejadnik, H.; Ye, D.; Lenkov, O. D.; Donig, J. S.; Martin, J. E.; Castillo, R.; Derugin, N.; Sennino, B.; Rao, J.; Daldrup-Link, H. Magnetic Resonance Imaging of Stem Cell Apoptosis in Arthritic Joints with a Caspase Activatable Contrast Agent. *ACS Nano* **2015**, *9* (2), 1150–1160.

(93) Wang, Y.; Hu, X.; Weng, J.; Li, J.; Fan, Q.; Zhang, Y.; Ye, D. A Photoacoustic Probe for the Imaging of Tumor Apoptosis by Caspase-Mediated Macrocyclization and Self-Assembly. *Angew. Chem., Int. Ed.* **2019**, *58* (15), 4886–4890.

(94) von Maltzahn, G.; Harris, T. J.; Park, J.-H.; Min, D.-H.; Schmidt, A. J.; Sailor, M. J.; Bhatia, S. N. Nanoparticle Self-Assembly Gated by Logical Proteolytic Triggers. *J. Am. Chem. Soc.* **2007**, *129* (19), 6064–6065.

(95) Ding, Z.; Sun, H.; Ge, S.; Cai, Y.; Yuan, Y.; Hai, Z.; Tao, T.; Hu, J.; Hu, B.; Wang, J.; Liang, G. Furin-Controlled Fe<sub>3</sub>O<sub>4</sub> Nanoparticle Aggregation and 19F Signal “Turn-On” for Precise MR Imaging of Tumors. *Adv. Funct. Mater.* **2019**, *29* (43), 1903860.

(96) Yuan, Y.; Ding, Z.; Qian, J.; Zhang, J.; Xu, J.; Dong, X.; Han, T.; Ge, S.; Luo, Y.; Wang, Y.; Zhong, K.; Liang, G. Casp3/7-Instructed Intracellular Aggregation of Fe<sub>3</sub>O<sub>4</sub> Nanoparticles Enhances T2MR Imaging of Tumor Apoptosis. *Nano Lett.* **2016**, *16* (4), 2686–2691.

(97) Wang, Y.; Li, X.; Chen, P.; Dong, Y.; Liang, G.; Yu, Y. Enzyme-instructed self-aggregation of Fe<sub>3</sub>O<sub>4</sub> nanoparticles for enhanced MRI T2 imaging and photothermal therapy of tumors. *Nanoscale* **2020**, *12* (3), 1886–1893.

(98) Stewart, P. S.; Costerton, J. W. Antibiotic resistance of bacteria in biofilms. *Lancet* **2001**, *358* (9276), 135–138.

(99) Li, L.-L.; Ma, H.-L.; Qi, G.-B.; Zhang, D.; Yu, F.; Hu, Z.; Wang, H. Pathological-Condition-Driven Construction of Supramolecular Nanoassemblies for Bacterial Infection Detection. *Adv. Mater.* **2016**, *28* (2), 254–262.

(100) Li, L.-L.; Zeng, Q.; Liu, W.-J.; Hu, X.-F.; Li, Y.; Pan, J.; Wan, D.; Wang, H. Quantitative Analysis of Caspase-1 Activity in Living Cells Through Dynamic Equilibrium of Chlorophyll-Based Nanoassembly Modulated Photoacoustic Signals. *ACS Appl. Mater. Interfaces* **2016**, *8* (28), 17936–17943.

(101) Cai, Q.; Fei, Y.; Hu, L.; Huang, Z.; Li, L.-L.; Wang, H. Chemotaxis-Instructed Intracellular Staphylococcus aureus Infection Detection by a Targeting and Self-Assembly Signal-Enhanced Photoacoustic Probe. *Nano Lett.* **2018**, *18* (10), 6229–6236.

(102) Lu, S.-Z.; Guo, X.-Y.; Zou, M.-S.; Zheng, Z.-Q.; Li, Y.-C.; Li, X.-D.; Li, L.-L.; Wang, H. Bacteria-Instructed In Situ Aggregation of AuNPs with Enhanced Photoacoustic Signal for Bacterial Infection Bioimaging. *Adv. Healthcare Mater.* **2020**, *9* (1), 1901229.

(103) Mizushima, N. Autophagy: process and function. *Genes Dev.* **2007**, *21* (22), 2861–73.

(104) Levine, B.; Kroemer, G. Autophagy in the pathogenesis of disease. *Cell* **2008**, *132* (1), 27–42.

(105) Mizushima, N.; Levine, B.; Cuervo, A. M.; Klionsky, D. J. Autophagy fights disease through cellular self-digestion. *Nature* **2008**, *451* (7182), 1069–75.

(106) Deretic, V.; Saitoh, T.; Akira, S. Autophagy in infection, inflammation and immunity. *Nat. Rev. Immunol.* **2013**, *13* (10), 722–37.

(107) Quarles, E. K.; Dai, D.-F.; Tocchi, A.; Basisty, N.; Gitari, L.; Rabinovitch, P. S. Quality control systems in cardiac aging. *Ageing Res. Rev.* **2015**, *23*, 101–115.

(108) Lin, Y.-X.; Qiao, S.-L.; Wang, Y.; Zhang, R.-X.; An, H.-W.; Ma, Y.; Rajapaksha, R. P. Y. J.; Qiao, Z.-Y.; Wang, L.; Wang, H. An in Situ Intracellular Self-Assembly Strategy for Quantitatively and Temporally Monitoring Autophagy. *ACS Nano* **2017**, *11* (2), 1826–1839.

(109) Qiao, S.-L.; Ma, Y.; Wang, Y.; Lin, Y.-X.; An, H.-W.; Li, L.-L.; Wang, H. General Approach of Stimuli-Induced Aggregation for Monitoring Tumor Therapy. *ACS Nano* **2017**, *11* (7), 7301–7311.

(110) Wang, S.; Huang, P.; Chen, X. Hierarchical Targeting Strategy for Enhanced Tumor Tissue Accumulation/Retention and Cellular Internalization. *Adv. Mater.* **2016**, *28* (34), 7340–64.

(111) Tanaka, A.; Fukuoka, Y.; Morimoto, Y.; Honjo, T.; Koda, D.; Goto, M.; Maruyama, T. Cancer Cell Death Induced by the Intracellular Self-Assembly of an Enzyme-Responsive Supramolecular Gelator. *J. Am. Chem. Soc.* **2015**, *137* (2), 770–775.

(112) Kim, C.; Kim, B. Anti-Cancer Natural Products and Their Bioactive Compounds Inducing ER Stress-Mediated Apoptosis: A Review. *Nutrients* **2018**, *10* (8), 1021.

(113) Wang, M.; Law, M. E.; Castellano, R. K.; Law, B. K. The unfolded protein response as a target for anticancer therapeutics. *Crit. Rev. Oncol. Hematol.* **2018**, *127*, 66–79.

(114) Fiandalo, M. V.; Kyprianou, N. Caspase control: protagonists of cancer cell apoptosis. *Exp. Oncol.* **2012**, *34* (3), 165–175.

(115) Hetz, C.; Mollereau, B. Disturbance of endoplasmic reticulum proteostasis in neurodegenerative diseases. *Nat. Rev. Neurosci.* **2014**, *15* (4), 233–249.

(116) Nakagawa, T.; Zhu, H.; Morishima, N.; Li, E.; Xu, J.; Yankner, B. A.; Yuan, J. Caspase-12 mediates endoplasmic-reticulum-specific apoptosis and cytotoxicity by amyloid-beta. *Nature* **2000**, *403* (6765), 98–103.

(117) Fu, C.; Zhan, J.; Huai, J.; Ma, S.; Li, M.; Chen, G.; Chen, M.; Cai, Y.; Ou, C. Furin-instructed molecular self-assembly actuates endoplasmic reticulum stress-mediated apoptosis for cancer therapy. *Nanoscale* **2020**, *12* (22), 12126–12132.

(118) Kalafatovic, D.; Nobis, M.; Javid, N.; Frederix, P. W. J. M.; Anderson, K. I.; Saunders, B. R.; Ulijn, R. V. MMP-9 triggered micelle-to-fibre transitions for slow release of doxorubicin. *Biomater. Sci.* **2015**, *3* (2), 246–249.

(119) Kalafatovic, D.; Nobis, M.; Son, J.; Anderson, K. I.; Ulijn, R. V. MMP-9 triggered self-assembly of doxorubicin nanofiber depots halts tumor growth. *Biomaterials* **2016**, *98*, 192–202.

(120) He, H.; Wang, J.; Wang, H.; Zhou, N.; Yang, D.; Green, D. R.; Xu, B. Enzymatic Cleavage of Branched Peptides for Targeting Mitochondria. *J. Am. Chem. Soc.* **2018**, *140* (4), 1215–1218.

(121) Yuan, Y.; Wang, L.; Du, W.; Ding, Z.; Zhang, J.; Han, T.; An, L.; Zhang, H.; Liang, G. Intracellular Self-Assembly of Taxol Nanoparticles for Overcoming Multidrug Resistance. *Angew. Chem., Int. Ed.* **2015**, *54* (33), 9700–4.

(122) Yuan, Y.; Zhang, J.; Qi, X.; Li, S.; Liu, G.; Siddhanta, S.; Barman, I.; Song, X.; McMahon, M. T.; Bulte, J. W. M. Furin-mediated intracellular self-assembly of olsalazine nanoparticles for enhanced magnetic resonance imaging and tumour therapy. *Nat. Mater.* **2019**, *18* (12), 1376–1383.

(123) Nguyen, M. M.; Carlini, A. S.; Chien, M. P.; Sonnenberg, S.; Luo, C.; Braden, R. L.; Osborn, K. G.; Li, Y.; Gianneschi, N. C.; Christman, K. L. Enzyme-Responsive Nanoparticles for Targeted Accumulation and Prolonged Retention in Heart Tissue after Myocardial Infarction. *Adv. Mater.* **2015**, *27* (37), 5547–52.

(124) Callmann, C. E.; Barback, C. V.; Thompson, M. P.; Hall, D. J.; Mattrey, R. F.; Gianneschi, N. C. Therapeutic Enzyme-Responsive Nanoparticles for Targeted Delivery and Accumulation in Tumors. *Adv. Mater.* **2015**, *27* (31), 4611–4615.

(125) Ai, X.; Ho, C. J. H.; Aw, J.; Attia, A. B. E.; Mu, J.; Wang, Y.; Wang, X.; Wang, Y.; Liu, X.; Chen, H.; Gao, M.; Chen, X.; Yeow, E. K. L.; Liu, G.; Olivo, M.; Xing, B. In vivo covalent cross-linking of photon-converted rare-earth nanostructures for tumour localization and theranostics. *Nat. Commun.* **2016**, *7* (1), 10432.

(126) Zhang, D.; Qi, G.-B.; Zhao, Y.-X.; Qiao, S.-L.; Yang, C.; Wang, H. In Situ Formation of Nanofibers from Purpurin18-Peptide Conjugates and the Assembly Induced Retention Effect in Tumor Sites. *Adv. Mater.* **2015**, *27* (40), 6125–6130.

(127) Qi, G.-B.; Zhang, D.; Liu, F.-H.; Qiao, Z.-Y.; Wang, H. An "On-Site Transformation" Strategy for Treatment of Bacterial Infection. *Adv. Mater. (Weinheim, Ger.)* **2017**, *29* (36), 1703461.

(128) Le Bonniec, B. F. Thrombin. In *Handbook of Proteolytic Enzymes*, Vol. 3; Rawlings, N. D., Salvesen, G., Eds.; Academic Press, 2013; Chapter 643, pp 2915–2932, DOI: [10.1016/B978-0-12-382219-2.00643-8](https://doi.org/10.1016/B978-0-12-382219-2.00643-8).

(129) Bremmer, S. C.; Chen, J.; McNeil, A. J.; Soellner, M. B. A general method for detecting protease activity via gelation and its application to artificial clotting. *Chem. Commun.* **2012**, *48* (44), 5482–5484.

(130) Chen, Q.; Wang, C.; Zhang, X.; Chen, G.; Hu, Q.; Li, H.; Wang, J.; Wen, D.; Zhang, Y.; Lu, Y.; Yang, G.; Jiang, C.; Wang, J.; Dotti, G.; Gu, Z. In situ sprayed bioresponsive immunotherapeutic gel for post-surgical cancer treatment. *Nat. Nanotechnol.* **2019**, *14* (1), 89–97.